

~~CONFIDENTIAL~~

AD372287

Export Control

ENERGY-MANEUVERABILITY (U)

AIR PROVING GROUND CENTER EGLIN AFB FL

MAR 1966

Distribution: Further dissemination only as directed by Air Proving Ground Center, Eglin AFB, FL, MAR 1966, or higher DoD authority. This document contains export-controlled technical data.

DECLASSIFIED UNDER AUTHORITY OF THE
INTERAGENCY SECURITY CLASSIFICATION APPEALS PANEL.
E.O. 13526, SECTION 5.3(b)(3)
ISCAP No. 2011-052, Document 1 Date March 13, 2013

10-MDR-125

~~CONFIDENTIAL~~

~~CONFIDENTIAL~~

Export Control

Redistribution Of DTIC-Supplied Information Notice

All information received from DTIC, not clearly marked "for public release" may be used only to bid on or to perform work under a U.S. Government contract or grant for purposes specifically authorized by the U.S. Government agency that is sponsoring access OR by U.S. Government employees in the performance of their duties.

Information not clearly marked "for public release" may not be distributed on the public/open Internet in any form, published for profit or offered for sale in any manner.

Non-compliance could result in termination of access.

Reproduction Quality Notice

DTIC's Technical Reports collection spans documents from 1900 to the present. We employ 100 percent quality control at each stage of the scanning and reproduction process to ensure that our document reproduction is as true to the original as current scanning and reproduction technology allows. However, occasionally the original quality does not allow a better copy.

If you are dissatisfied with the reproduction quality of any document that we provide, please free to contact our Directorate of User Services at (703) 767-9066/9068 or DSN 427-9066/9068 for refund or replacement.

Do Not Return This Document To DTIC

~~CONFIDENTIAL~~

UNCLASSIFIED

AD NUMBER
AD372287
CLASSIFICATION CHANGES
TO
confidential
FROM
secret
AUTHORITY
OCA & GP-3, Mar 1978

THIS PAGE IS UNCLASSIFIED

The following notice applies to any unclassified (including originally classified and now declassified) technical reports released to "qualified U.S. contractors" under the provisions of DoD Directive 5230.25, Withholding of Unclassified Technical Data From Public Disclosure.

NOTICE TO ACCOMPANY THE DISSEMINATION OF EXPORT-CONTROLLED TECHNICAL DATA

1. Export of information contained herein, which includes, in some circumstances, release to foreign nationals within the United States, without first obtaining approval or license from the Department of State for items controlled by the International Traffic in Arms Regulations (ITAR), or the Department of Commerce for items controlled by the Export Administration Regulations (EAR), may constitute a violation of law.
2. Under 22 U.S.C. 2778 the penalty for unlawful export of items or information controlled under the ITAR is up to ten years imprisonment, or a fine of \$1,000,000, or both. Under 50 U.S.C., Appendix 2410, the penalty for unlawful export of items or information controlled under the EAR is a fine of up to \$1,000,000, or five times the value of the exports, whichever is greater; or for an individual, imprisonment of up to 10 years, or a fine of up to \$250,000, or both.
3. In accordance with your certification that establishes you as a "qualified U.S. Contractor", unauthorized dissemination of this information is prohibited and may result in disqualification as a qualified U.S. contractor, and may be considered in determining your eligibility for future contracts with the Department of Defense.
4. The U.S. Government assumes no liability for direct patent infringement, or contributory patent infringement or misuse of technical data.
5. The U.S. Government does not warrant the adequacy, accuracy, currency, or completeness of the technical data.
6. The U.S. Government assumes no liability for loss, damage, or injury resulting from manufacture or use for any purpose of any product, article, system, or material involving reliance upon any or all technical data furnished in response to the request for technical data.
7. If the technical data furnished by the Government will be used for commercial manufacturing or other profit potential, a license for such use may be necessary. Any payments made in support of the request for data do not include or involve any license rights.
8. A copy of this notice shall be provided with any partial or complete reproduction of these data that are provided to qualified U.S. contractors.

DESTRUCTION NOTICE

For classified documents, follow the procedure in DoD 5220.22-M, National Industrial Security Program, Operating Manual, Chapter 5, Section 7, or DoD 5200.1-R, Information Security Program Regulation, Chapter 6, Section 7. For unclassified, limited documents, destroy by any method that will prevent disclosure of contents or reconstruction of the document.

SECURITY

MARKING

The classified or limited status of this report applies to each page, unless otherwise marked.

Separate page printouts MUST be marked accordingly.

THIS DOCUMENT CONTAINS INFORMATION AFFECTING THE NATIONAL DEFENSE OF THE UNITED STATES WITHIN THE MEANING OF THE ESPIONAGE LAWS, TITLE 18, U.S.C., SECTIONS 793 AND 794. THE TRANSMISSION OR THE REVELATION OF ITS CONTENTS IN ANY MANNER TO AN UNAUTHORIZED PERSON IS PROHIBITED BY LAW.

NOTICE: When government or other drawings, specifications or other data are used for any purpose other than in connection with a definitely related government procurement operation, the U. S. Government thereby incurs no responsibility, nor any obligation whatsoever; and the fact that the Government may have formulated, furnished, or in any way supplied the said drawings, specifications, or other data is not to be regarded by implication or otherwise as in any manner licensing the holder or any other person or corporation, or conveying any rights or permission to manufacture, use or sell any patented invention that may in any way be related thereto.

REPRODUCTION QUALITY NOTICE

This document is the best quality available. The copy furnished to DTIC contained pages that may have the following quality problems:

- Pages smaller or larger than normal.
- Pages with background color or light colored printing.
- Pages with small type or poor printing; and or
- Pages with continuous tone material or color photographs.

Due to various output media available these conditions may or may not cause poor legibility in the microfiche or hardcopy output you receive.

If this block is checked, the copy furnished to DTIC contained pages with color printing, that when reproduced in Black and White, may change detail of the original copy.

[REDACTED]

ENERGY-MANEUVRABILITY (U)

by

John R. Boyd, Maj, USAF
Thomas P. Christie
James E. Gibson, 1st Lt, USAF

**SPECIAL HANDLING REQUIRED
NOT RELEASABLE TO
FOREIGN NATIONALS**
The information contained in this document
will not be disclosed to foreign nationals or
their representatives.

This material contains information affecting
the national defense of the United States
within the meaning of the Espionage Laws
(Title 18, U.S.C., sections 793 and 794), the
transmission or revelation of which in any
manner to an unauthorized person is pro-
hibited by law.

In addition to security requirements which must
be met, this document is subject to special ex-
port controls and each transmittal to foreign
governments or foreign nationals may be made
only with prior approval of ANGC (PGTO) Eglin
AFB, Florida

**GROUP-3
DOWNGRADED AT 12 YEAR INTERVALS;
NOT AUTOMATICALLY DECLASSIFIED.**

[REDACTED]

(This page is Unclassified)

FOREWORD

(U) This report on Project 0350T4 will be published in three volumes. Volume I contains the theory, sample application, and the associated mathematical model. This effort commenced on 15 June 1965 and was completed on 15 January 1966. Volumes II and III will contain a few sample comparative analyses and the Energy-Maneuverability Diagrams of several aircraft for clean and air-to-air configurations. This report supersedes APGC-TDR-64-35 (reference 8).

(U) The magnitude of this program precludes the listing of all individuals whose efforts have been invaluable to the progress of the work and the preparation of this report. However, special recognition must be given to Mr. Carl Davy, Mathematician, and Mrs. Anthony Biele, Programmer, of the Mathematical Services Laboratory, and to Miss Betty Jo Salter, Illustrator, of the Graphics Section.

This technical report has been reviewed and is approved.

Walter P. Glover

WALTER P. GLOVER, Colonel, USAF
Director, Air Force Armament Laboratory

J. E. Roberts

J. E. ROBERTS, Major General, USAF
Commander, Air Proving Ground Center

UNCLASSIFIED ABSTRACT

This report shows how an aircraft's energy state and energy rate capabilities are directly related to operational maneuverability and efficiency in terms of energy-maneuverability theory. It demonstrates also how energy-maneuverability theory may be applied to assist the tactician, commander, planner, and designer in optimizing aircraft performance. Load factor versus velocity (G-V) and altitude versus Mach number (H-M) diagrams are employed to obtain the interacting energy relationships fundamental to energy-maneuverability theory. The G-V diagrams provide a measure of instantaneous maneuverability while the H-M diagrams (the most valuable diagrams) show sustained maneuverability as a function of energy rate, g , efficiency, and range throughout an aircraft's performance envelope. The energy diagrams, as the working tools of energy-maneuverability theory, may be used to determine operational maneuverability and efficiency of various armament-engine-airframe combinations.

This document is subject to special export controls and each transmittal to foreign governments or foreign nationals may be made only with prior approval of APOG (PGTO), Eglin AFB, Florida.

CONTENTS

Section		Page
I.	INTRODUCTION	1
II.	INSTANTANEOUS MANEUVERABILITY	2
III.	SUSTAINED MANEUVERABILITY	4
	General	4
	Energy Rate	6
	G	8
	Efficiency	10
	Range	13
IV.	TACTICAL APPLICATIONS	15
V.	REQUIREMENTS	31
	REFERENCES	78

Appendix

I.	RULE-OF-THUMB PERFORMANCE CAPABILITY OF AIM-7E AND AIM-9B/ AA-2 MISSILES	32
II.	MATHEMATICAL DERIVATIONS AND MODELS FOR DEVELOPING ENERGY- MANEUVERABILITY THEORY AND ASSOCIATED FLIGHT PATHS	39
III.	A COMPARISON OF THE BRYSON-KELLEY AND THE MODIFIED RUTOWSKI TECHNIQUES	74

NASIC/ACAA
 DECLASSIFY
 (This information no
 longer
 needs to be
 classified)

ILLUSTRATIONS AND TABLES

Figure

1.	F-4C G-V Diagram at 30,000 Feet	3
2.	F-4C Steady-State Envelope	5
3.	F-4C L-G Energy Rate Diagram with Superimposed Rutowski Minimum Time Path	7
4.	F-4C L-G Energy Rate Diagram with Superimposed Rule-of- Thumb Path	7
5.	F-4C 3-G Energy Rate Diagram	9
6.	F-4C 5-G Energy Rate Diagram	9
7.	Constant (50%) Fuel E-M Efficiency Diagram	12
8.	F-4C Variable Fuel E-M Efficiency Diagram	12
9.	F-4C Range Diagram	14
10.	F-4C G-V Diagram at 30,000 Feet	16
11.	MIG-21 G-V Diagram at 30,000 Feet	16

NASIC/ACAA
 DECLASSIFY
 (This information no
 longer
 needs to be classified)

CONTENTS (Continued)

NASIC/ACAA
DECLASSIFY
(This information
no longer
needs to be
classified)

13, 15, 17, 19, 21, 23,
25, 27, 29, 31, 33

Figure

Page

12.	F-4C Maximum Power 1-G Energy Rate Diagram	17
13.	MIG-21 Maximum Power 1-G Energy Rate Diagram	17
14.	F-4C Maximum Power 3-G Energy Rate Diagram	19
15.	MIG-21 Maximum Power 3-G Energy Rate Diagram	19
16.	F-4C Maximum Power 5-G Energy Rate Diagram	20
17.	MIG-21 Maximum Power 5-G Energy Rate Diagram	20
18.	F-4C Military Power 1-G Energy Rate Diagram	21
19.	MIG-21 Military Power 1-G Energy Rate Diagram	21
20.	F-4C Military Power 3-G Energy Rate Diagram	22
21.	MIG-21 Military Power 3-G Energy Rate Diagram	22
22.	F-4C Military Power 5-G Energy Rate Diagram	23
23.	MIG-21 Military Power 5-G Energy Rate Diagram	23
24.	F-4C Maximum Power Constant (50%) Fuel E-M Efficiency Diagram .	24
25.	MIG-21 Maximum Power Constant (50%) Fuel E-M Efficiency Diagram	24
26.	F-4C Maximum Power Variable Fuel E-M Efficiency Diagram	25
27.	MIG-21 Maximum Power Variable Fuel E-M Efficiency Diagram	25
28.	F-4C Military Power Constant (50%) Fuel E-M Efficiency Diagram	27
29.	MIG-21 Military Power Constant (50%) Fuel E-M Efficiency Diagram	27
30.	F-4C Military Power Variable Fuel E-M Efficiency Diagram	28
31.	MIG-21 Military Power Variable Fuel E-M Efficiency Diagram	28
32.	F-4C Range Diagram	29
33.	MIG-21 Range Diagram	29

Table

I.	Rutowski Minimum Time Paths (Maximum Power)	15
II.	Rutowski Minimum Time Paths (Military Power)	18
III.	Rutowski Minimum Fuel Paths (Maximum Power)	26
IV.	Rutowski Minimum Fuel Paths (Military Power)	26

SECTION I

INTRODUCTION

(U) Aircraft maneuverability can be defined as the ability to change direction and/or magnitude of the velocity vector. While this definition describes maneuverability accurately, it provides little feel for the fighter pilot or engineer on how to acquire best (optimum) maneuverability. However, from experience, we know that the best way to maneuver for position advantage or to deny this same advantage to an opponent depends on the type of ordnance used and the performance of the aircraft. The type of ordnance employed determines the possible delivery conditions needed to effectively deliver this ordnance, whether it be guided missiles, guns, or bombs. Quantitatively, these delivery conditions can be depicted by launch or firing envelopes. Once the initial delivery conditions are known, the problem becomes one of maneuvering into the effective launch envelope. Such maneuverability is dependent upon the ability of the pilot to control turn, altitude, airspeed, and acceleration.

(U) The purpose of the following discussion is to show how energy-maneuverability is related to operational maneuverability and how this relationship may be exploited by the tactician, commander, planner, or designer in developing valid maneuvering and/or delivery tactics along with better aerial combat weapons systems.

SECTION II

INSTANTANEOUS MANEUVERABILITY

(U) Turn can be described in terms of radius (r) and/or rate (ω) at various airspeeds (V) and radial g (N_r) by employing the relationships

$$r = \frac{V^2}{gN_r} \quad \text{and} \quad \omega = \frac{gN_r}{V}$$

in conjunction with aerodynamic force system equations. From such equations, numerous charts depicting turn radius and rate can be developed to provide some measure of maneuverability. Needless to say, the numerous charts and associated contours are difficult to digest. For simplification and clarity, load factor versus velocity (G-V) diagrams are employed to depict turn in a manner consistent with a pilot's background and his cockpit instrumentation. (See Figure 1.)

(U) The intent of this diagram (Figure 1) is to enable a pilot to determine maximum turn in terms of g or load factor by consulting the aerodynamic limit at the left and the structural/stabilator limits at the top, bottom, and to the right. By an overlay comparison of G-V diagrams, a pilot can determine if he, or a possible adversary, has a turn advantage. Any turn capability or advantage, extracted from such a diagram, provides only a relative measure of instantaneous maneuverability. The diagram fails to indicate the effect of pulling g in terms of losing or gaining altitude and/or airspeed. As a result, no measure of sustained maneuverability can be acquired from a study of this diagram. To develop this information, a look in a different direction is necessary.

~~CONFIDENTIAL~~

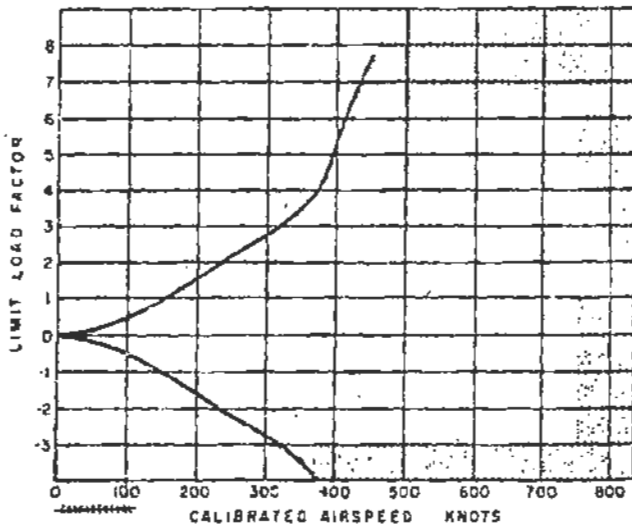


Figure 1. F-4C G-V Diagram at 30,000 Feet.

~~CONFIDENTIAL~~

~~CONFIDENTIAL~~

SECTION III

SUSTAINED MANEUVERABILITY

GENERAL

(U) Altitude, airspeed, and changes thereto are directly dependent upon the force system acting along, and normal to, the flight path. By mathematically manipulating the expressions describing this force system, altitude (h) and airspeed (V) can be combined in the expression for specific energy (E_s);

$$E_s = h + \frac{V^2}{2g},$$

as shown in Appendix II.

(U) To maneuver for a desired change or a combination of changes in direction, altitude, and airspeed, a pilot must disturb the force system surrounding his aircraft. Therefore, from the above expression, we deduce that maneuverability is not only related to directional change (turn), but is also related to specific energy in terms of altitude and airspeed. From this expression, we can also deduce that all maneuvering will be conducted between a maximum energy level associated with a best altitude-airspeed combination and a minimum energy level associated with zero altitude and minimum airspeed. These maximum and minimum energy levels may be represented in an altitude versus Mach number (H-M) diagram (Figure 2). The maximum energy level is located on Figure 2 at the point where the specific energy (E_s) contour is tangent to the steady-state envelope. The minimum energy level is located on Figure 2 at sea level where the appropriate specific energy contour intercepts the steady-state envelope. (The steady-state envelope is defined as the level flight operating boundary determined by angle-of-attack limits, thrust available, drag, and structural limits.)

(U) In an air-to-air battle, offensive maneuvering advantage will belong to the pilot who can enter an engagement at a higher energy level and maintain more energy than his opponent while locked in a maneuver and counter-maneuver duel. Maneuvering advantage will also belong to the pilot who enters an air-to-air battle at a lower energy level, but can gain more energy than his opponent during the course of the battle. From a performance standpoint, such an advantage is clear because the pilot with the most energy has a better opportunity to engage or disengage at his own choosing. On the other hand, energy-loss maneuvers can be employed defensively to nullify an attack or to gain a temporary offensive maneuvering position. Implicit in the entire

4
~~CONFIDENTIAL~~

(This page is unclassified)

~~CONFIDENTIAL~~

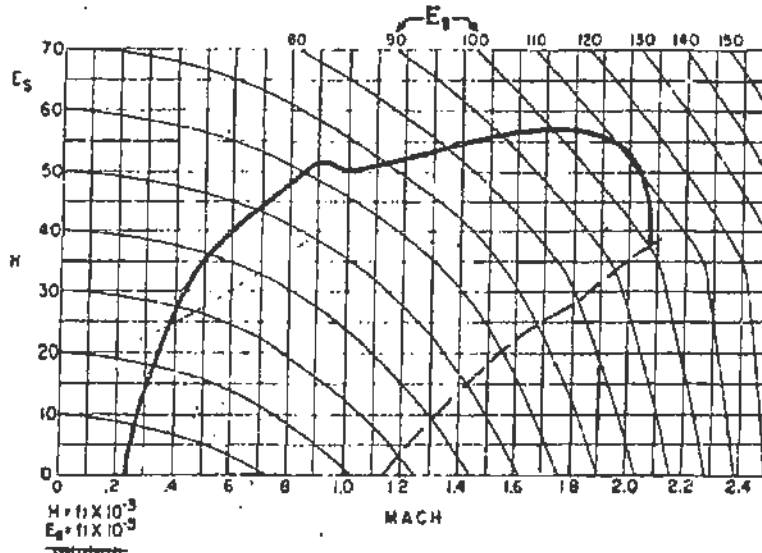


Figure 2. F-4C Steady-State Envelope.

discussion on energy state and/or energy rate advantages is the fact that a pilot has enough internal energy (fuel) available to exploit these advantages.

(U) In an air-to-surface role, a pilot is not as interested in a high energy state as he is in maintaining energy while maneuvering with a wide assortment of stores on board. If he cannot maintain maneuvering energy, his choice of tactics/techniques becomes limited. In addition, if this same pilot is tapped by enemy air, his ability to evade or nullify the attack becomes questionable.

(U) Observing the correlation of energy with maneuverability, it follows that tactical maneuverability is related to the amount of energy possessed and how well that energy is managed. From a design standpoint, this means a fighter pilot must be given a vehicle wherein such factors as energy state, energy rate, and the quantity of internal energy available are properly considered. For best maneuverability, the fighter pilot must know when and how to move to a higher or lower energy level and how to best conserve his internal energy when locked in an air-to-air or air-to-surface encounter.

~~CONFIDENTIAL~~

~~CONFIDENTIAL~~

ENERGY RATE

(U) For an offensive maneuvering advantage, a fighter pilot must be at a higher energy level or be able to gain energy more quickly than his adversary before the maneuver and counter-maneuver portion of the battle begins. To gain energy more quickly—once GCI, radar, or visual contact is made—necessitates a best path for accomplishing this task.

(U) An approximate method for finding a best flight path was discovered by E. S. Rutowski (see Reference 1). Using his method, as outlined in Appendix II, the best (Rutowski) path for gaining maneuvering energy may be represented on an altitude versus Mach number (H-M) diagram containing energy rate (specific excess power) contours within the steady-state envelope, as shown in Figure 3. Energy gain is maximum at the points where the specific energy (E_s) contours are tangent to the specific excess power (P_s) contours, where

$$P_s = \left(\frac{T_a - D}{W} \right) V,$$

T_a = thrust available, D = drag, V = velocity, and W = weight. A glance at Figure 3 shows a best (optimum) path for gaining energy most rapidly. Not normally shown is the best path when the starting point is located off the basic Rutowski path. A solution to this problem becomes easy if the energy rate, off the Rutowski path, inside the steady-state envelope is assumed to be zero. Under this assumption, the pilot moves along the specific energy contour consistent with his energy level until intercept is made with the Rutowski path. As shown in Figure 3, the best path consists of two segments: the appropriate specific energy contour and the basic Rutowski path. Using this procedure, pilots can determine the best paths from any point in the envelope. However, these paths are approximate for two reasons: (1) load factor is assumed constant (1 g) in developing the basic Rutowski path and (2) energy rate is assumed to be zero in developing the best path from any point in the envelope.

(U) To provide a more exact solution, A. E. Bryson and H. J. Kelley (Reference 2 and Appendix II) have developed a direct method while H. P. Heermann (Reference 3) has developed an indirect method for finding best paths. Flight paths, determined by these methods, show that Rutowski is very nearly correct. Rutowski's method, when compared with the Bryson-Kelley and Heermann methods, reveals that a rule-of-thumb technique can be used by a pilot or engineer to find best energy paths. (See Appendix III.) The technique uses the simple rule $\Delta E_s = k\Delta H$ for finding intercept curves and the subsonic-supersonic transition curve to the Rutowski path. (See Figure 4.) The value of $k = 2/3$ when Mach number must be decreased and $k = -1$ when Mach number must be increased to intercept the basic Rutowski path.

CONFIDENTIAL

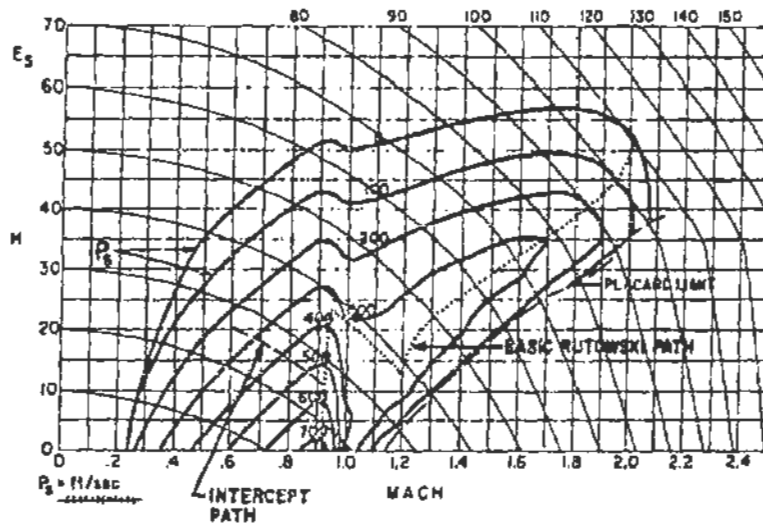


Figure 3. F-4C L-G Energy Rate Diagram with Superimposed Rutowski Minimum Time Path.

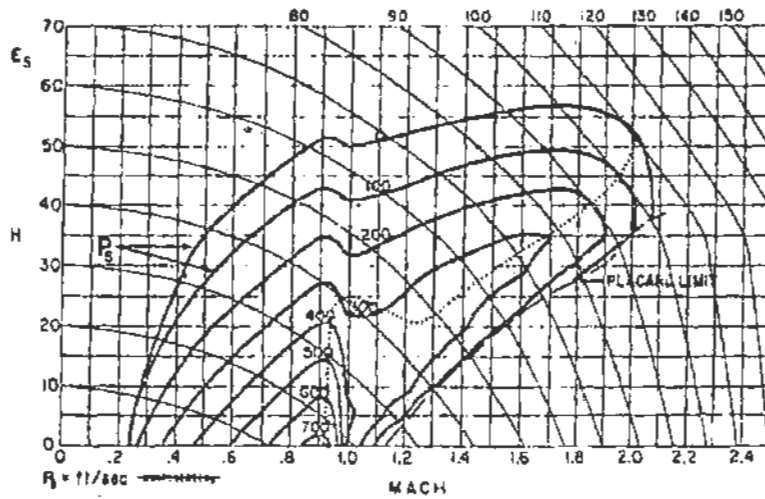


Figure 4. F-4C L-G Energy Rate Diagram with Superimposed Rule-of-Thumb Path.

7

CONFIDENTIAL

~~CONFIDENTIAL~~

(U) Even though the path developed by this procedure may be satisfactory to the engineer, it still is not good enough to enable the pilot to fly the path, because of the constantly changing altitude, Mach number, and pitch angle. Observation and analysis of the path just defined, however, suggest a way to avoid this predicament. Generally speaking, the subsonic portion of the path can be represented by a constant Mach number climb, while the supersonic portion may be approximated by an average constant calibrated airspeed. To intercept the subsonic or supersonic segments, the pilot pulls up or pushes over, as indicated by the rule-of-thumb, until he intercepts the basic path. At intercept, the pilot should lead the Mach number or calibrated airspeed to prevent a temporary loss of energy by pulling too much g. Intercepts from the subsonic segment to the supersonic segment of the Rutowski path should be accomplished at less than 2 g, while intercepts to the subsonic portion of the Rutowski path should be accomplished at less than 3 or 4 g at lower altitudes and should decrease correspondingly as altitude increases.

(U) Although the H-N diagram is useful for approximating best energy rate flight paths, observation reveals that it can also be used for another purpose. The contours contained within the steady-state envelope provide a measure of the ability to gain energy throughout the envelope. Since gaining energy is related to maintaining maneuverability, the L-g Energy Rate diagram provides a measure of sustained maneuverability as a function of energy rate. By overlay techniques, the L-g Energy Rate diagram can be used by the fighter pilot or tactician to determine if he can gain energy more quickly than some adversary. Actual time values, depicting how rapidly the transfer takes place, can be provided by the previously-mentioned optimization programs. Such values will be provided in "Tactical Applications," Section IV of this report. When this information is correlated with some analysis yet to be presented, the pilot or tactician can then determine the type of tactics or maneuvers to employ.

G

(U) Energy Rate diagrams of more than 1 g can be helpful in determining the best tactics to employ in the maneuver and counter-maneuver portions of the fight. As shown in Figures 5 and 6, these diagrams contain both positive and negative energy rate (P_e) contours within the steady-state envelope. As such, these diagrams portray the ability to maintain energy while pulling g; hence, they provide a measure of sustained maneuverability as a function of g.

(U) Once again, by simple overlay or comparison techniques, regions of energy advantage and disadvantage can be easily determined. If a fighter pilot can gain energy more quickly or lose it less rapidly than some adversary in a maneuvering fight, he has offensive maneuvering advantage. On the other hand,

8

~~CONFIDENTIAL~~

(This page is Unclassified)

~~CONFIDENTIAL~~

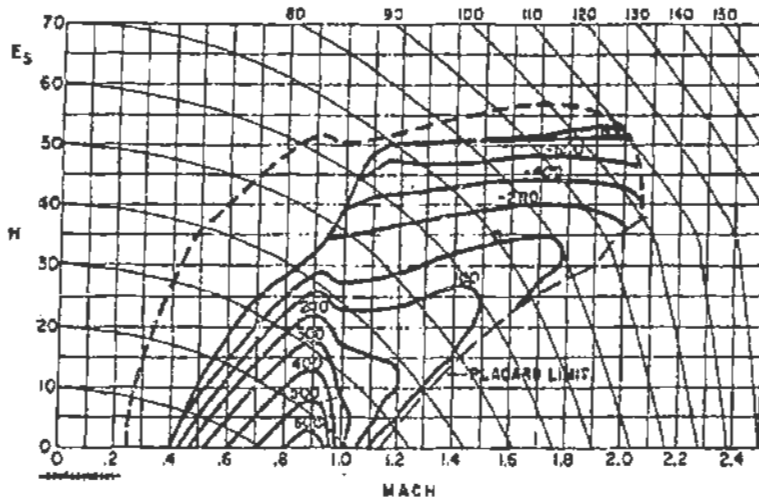


Figure 5. F-4C 3-G Energy Rate Diagram.

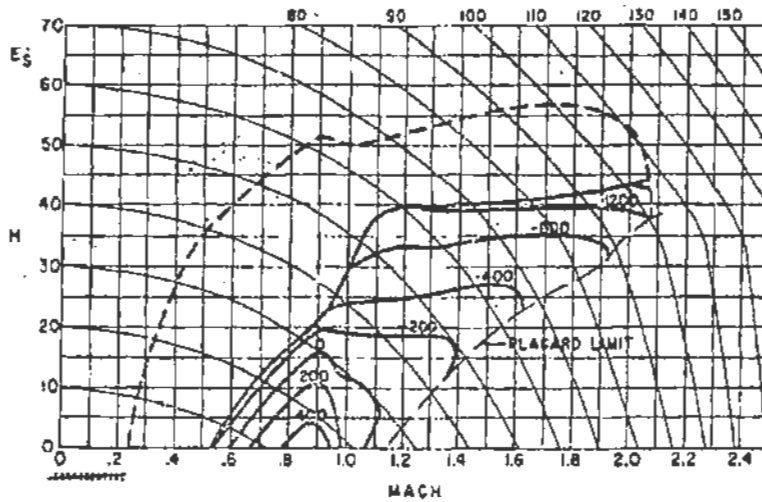


Figure 6. F-4C 5-G Energy Rate Diagram.

9
~~CONFIDENTIAL~~

~~CONFIDENTIAL~~

if the energy values are reversed, the pilot, although forced on the defensive, may employ energy loss maneuvers to his advantage. In either case, the 3-g and 5-g Energy Rate diagrams graphically portray capabilities and limitations in the maneuver and counter-maneuver portions of the fight. In the air-to-surface role, these diagrams may be employed to determine maneuvering capabilities and limitations with a wide assortment of stores on board. With this information, pilots and tacticians can develop pre-attack and post-attack tactics and maneuvers against a hostile surface complex.

(U) Even though the 3-g and 5-g diagrams serve as useful tools to determine advantages and disadvantages, they do not specify the exact tactics or maneuvers needed. To decide what maneuvers should be employed, a pilot must be well versed in the theory, and proficient in the practice, of air-to-air and air-to-surface tactics (see References 4 and 5). With this background, a pilot can translate relative energy gain or loss relationships into valuable tactical maneuvers.

(U) Recently, the Bryson-Kelley method has been employed to develop best three-dimensional maneuvers (see Reference 6). This method appears promising in finding specific optimum maneuvers for change of direction, rate of closure, and combinations thereof in minimum time or with minimum fuel until weapons launch. However, as presently developed, this method fails to consider: (1) the best relative regions within the flight envelope to maneuver and counter-maneuver against a known adversary; (2) plausible counter-maneuvers by an adversary as he observes and/or anticipates the optimum maneuvers; (3) a sequence of plausible counter-maneuvers or maneuvers by an adversary for which a sequence of optimum maneuvers or counter-maneuvers will be necessary; and (4) the possibility that more than one optimum maneuver or counter-maneuver can be flown against a specific counter-maneuver or maneuver.

(U) Because of these serious deficiencies, the Bryson-Kelley method cannot be used by itself to develop valid tactics for the air-to-air battle. However, there may be a possibility of developing near optimum tactics if the qualitative knowledge of the tactician concerning plausible maneuvers and counter-maneuvers is used in conjunction with the quantitative methods developed by Rutowski, Bryson-Kelley, and Heermann. The Deputy for Effectiveness Test, Air Proving Ground Center, and the Air Force Armament Laboratory, Research and Technology Division (ATD), Eglin Air Force Base, Florida, are investigating the use of these methods for this purpose.

EFFICIENCY

(U) Until now, the discussion has been concerned with energy state (h, V) and/or energy rate (P_e) in an effort to describe maneuverability and to gain ma-

~~CONFIDENTIAL~~

maneuvering advantage. Knowing that energy state and/or energy rate advantage depends upon the internal energy (fuel) available, we will now consider the amount of internal energy that can be converted into maneuvering energy. To acquire this information, a mathematical expression must be developed which considers specific energy gained versus internal energy expended. Such an expression is

$$E-ME = \frac{P^*}{W_f} w_f$$

where E-ME = energy-maneuverability efficiency, P^* = average specific excess power, W_f = fuel weight rate flow, and w_f = fuel weight. (See Appendix II for detailed development of this expression.) Two types of E-M Efficiency diagrams, incorporating these efficiency contours within the steady-state envelope, may be constructed. In the first diagram (see Figure 7) constant fuel weight (50% internal) is assumed. In the second diagram (see Figure 8) only the fuel remaining at a given energy level is considered, after reducing the quantity of fuel by the minimum amount of fuel needed to reach that energy level. The efficiency contours depicted on this diagram consider fuel available minus 5% internal fuel and 20 minutes fuel for best loiter speed at 10,000 ft. Both of these E-M Efficiency diagrams can be used to: (1) find the most efficient (minimum fuel) paths by employing the same rule-of-thumb techniques used with the Energy Rate diagrams and (2) determine the amount of internal energy that can be converted into maneuvering energy as well as the efficiency of that conversion. Since the diagrams can be employed in this fashion, they provide a measure of sustained maneuverability as a function of efficiency. In addition, E-M Efficiency diagrams can be used extensively to determine relative advantages and disadvantages of competing transport and bomber designs. For these type aircraft, load factor and energy rate are less important measures of operational performance. The second E-M Efficiency diagram is more meaningful, since variable fuel weight is considered throughout the flight envelope. However, the constant fuel E-M Efficiency diagram is important in determining regions of best efficiency, independent of fuel histories. The relative merit of these two diagrams will be discussed in "Tactical Applications," Section IV of this report.

(U) By employing comparative techniques, the tactician can generally see whether a fighter pilot or his adversary will conserve a greater percentage of fuel in moving from one energy level to another. Higher numerical values indicate a greater percentage of fuel remaining or a smaller percentage of fuel consumed. Thus, by correlating the E-M Efficiency diagrams with the Energy Rate diagrams, the tactician can determine to what degree a pilot or his adversary can realistically maintain or employ any energy state and/or energy rate advantages. To assist in this endeavor actual fuel percentage values can be provided (by the optimization programs) to show how efficiently the

~~CONFIDENTIAL~~

(This page is Unclassified)

CONFIDENTIAL

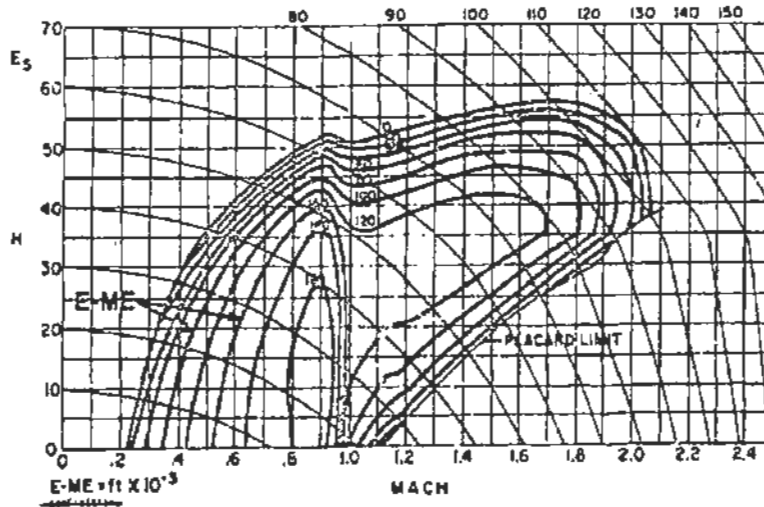


Figure 7. Constant (50%) Fuel E-M Efficiency Diagram.

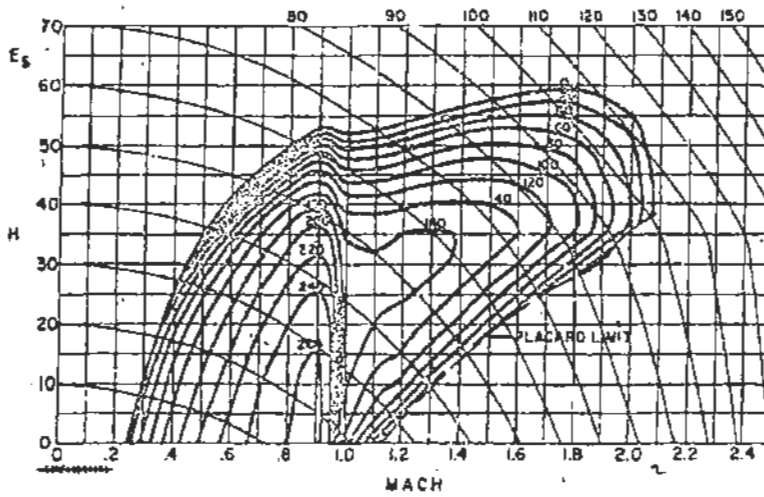


Figure 8. F-4C Variable Fuel E-M Efficiency Diagram.

CONFIDENTIAL

~~CONFIDENTIAL~~

energy transfer takes place. Such information will be provided in "Tactical Applications," Section IV of this report.

RANGE

(U) Thus far, maneuverability has been described directly as a function of energy rate, g , and efficiency. However, to completely describe maneuverability, we must consider indirect as well as direct influences. Range indirectly influences maneuverability as it plays a vital part in determining the area of maneuverability available over the earth's surface. Because of this relationship, a combat pilot must have a good but simple measure of his available range at any altitude-airspeed combination within the steady-state envelope. To gain this information, we must consider: (1) the fuel consumed and the distance traversed in reaching any altitude-airspeed combination and (2) the remaining range available as a function of the fuel remaining at any altitude-airspeed combination.

(U) By properly considering this information, as outlined in Appendix II, an H-M diagram depicting range can be developed (see Figure 9). From this diagram a pilot can determine range at any altitude-airspeed combination including the distance traversed to reach that combination. The range contours depicted on this diagram are based on the same fuel reserve considerations used in the variable fuel E-M Efficiency diagram. The shaded area on the chart represents a transient region in the flight envelope. In this region, aircraft drag, i.e., thrust required, is greater than military thrust available and less than minimum afterburner thrust. For this reason, steady-state flight is not possible unless some device, e.g., speedbrakes, is employed to increase drag.

(U) By using the Range diagram in conjunction with the other energy-maneuverability diagrams, the tactician can determine to what degree a pilot or his adversary can realistically gain advantage consistent with distance from friendly airfields or tanker support. In addition, planners and designers can evaluate the true operational performance of transport and bomber type aircraft by considering the Range diagram along with the E-M Efficiency diagrams.

~~CONFIDENTIAL~~

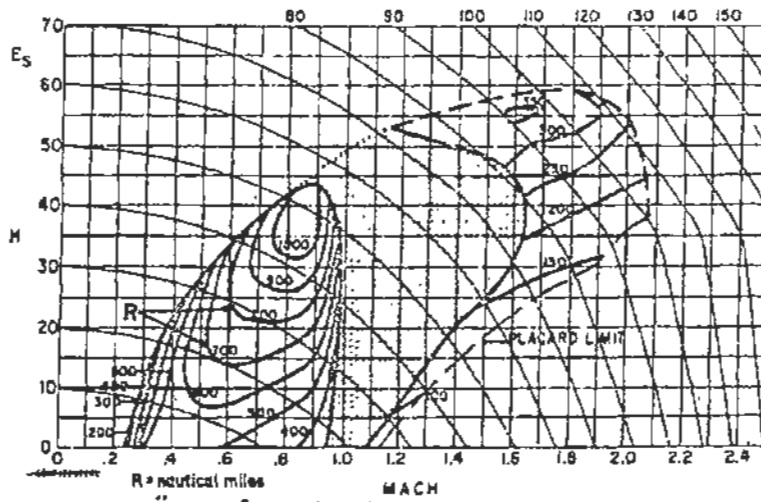


Figure 9. F-4C Range Diagram.

~~CONFIDENTIAL~~

SECRET

SECTION IV

TACTICAL APPLICATIONS

(U) If the energy-maneuverability concept is incorporated in the present knowledge on fighter tactics, a pilot can be provided more meaningful information on how he should maneuver to gain advantage. The resulting information will then reveal to the pilot how he should best exploit the maneuvering capabilities of his aircraft. Additionally, valid comparative analyses can be performed if similar diagrams are constructed for potential enemy fighters. The relative regions of advantage or disadvantage are found in terms of g, energy rate, efficiency, and range by performance comparisons throughout the flight envelope. From this comparison, the tactician or pilot can easily determine which of two aircraft has the advantage in terms of instantaneous maneuverability, sustained maneuverability, and range. Using this information, the tactician can determine how to best maneuver for advantage.

(S) For a sample comparison, we shall consider the F-4C versus the Soviet MIG-21 and determine maneuvering advantages and disadvantages. The conditions for comparison will be typical air-to-air configurations, with 50% internal fuel, unless specified otherwise. In the G-V diagrams (Figures 10 and 11), the aerodynamic g limit of the MIG-21 lies to the left of the same limit for the F-4C. At a glance, Figures 10 and 11 indicate the MIG-21 has an enormous instantaneous maneuverability advantage over the F-4C. These diagrams also indicate that the MIG-21 has an advantage when comparing structural limits. The 1-g Energy Rate diagrams (Figures 12 and 13) show that the MIG-21 has the advantage within most of the subsonic portion of the flight envelope and throughout all of the supersonic portion of the flight envelope. The only region of advantage for the F-4C lies in the subsonic and transonic areas below 15,000 feet. The magnitude of the maximum power energy rate advantage can be determined by consulting Table I.

NASIC/ACAA
DECLASSIFY
(This
information no
longer
needs to be
classified)

TABLE I. RUTOWSKI MINIMUM TIME PATHS (MAXIMUM POWER)

Type Aircraft	$E_2 = 3,000$ ft to $E_1 = 70,000$ ft			$E_2 = 3,000$ ft to $E_1 = 95,000$ ft		
	Time (sec)	Fuel Weight Used (lb)	Fuel Used (%)	Time (sec)	Fuel Weight Used (lb)	Fuel Used (%)
F-4C	197	3655	32	325	5487	48
MIG-21	187	1586	36	247	1801	42

SECRET

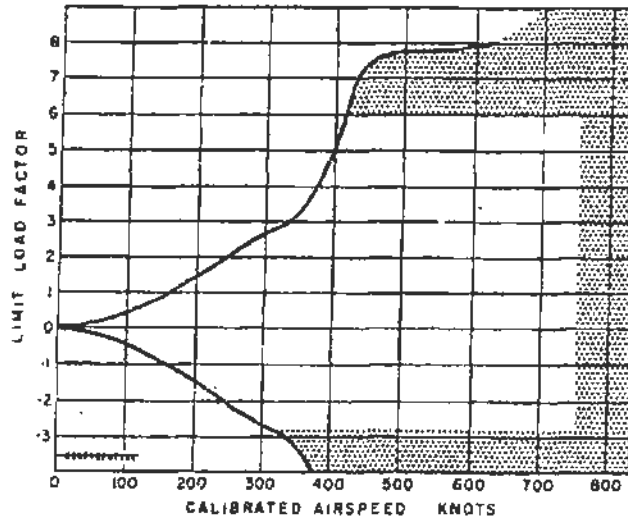


Figure 10. F-4C G-V Diagram at 30,000 Feet.

NASIC/ACAA
DECLASSIFY
(This information no
longer
needs to be classified)

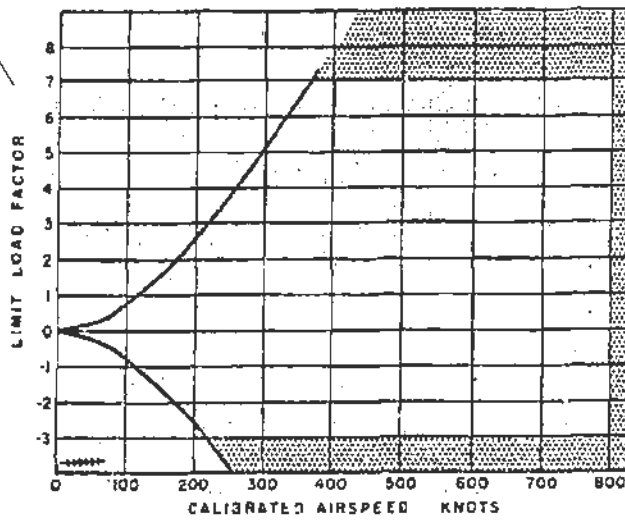


Figure 11. MIG-21 G-V Diagram at 30,000 Feet.

SECRET

SECRET

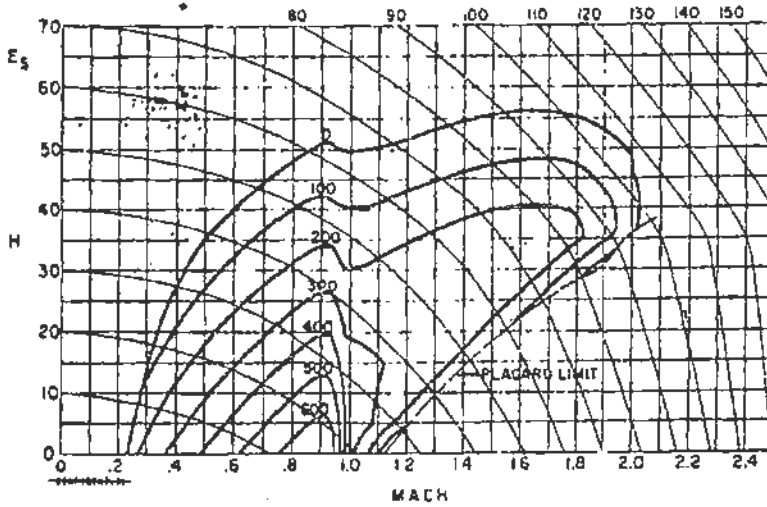


Figure 12. P-4C Maximum Power 1-3 Energy Rate Diagram.

NASIC/ACAA
DECLASSIFY
(This information no
longer
needs to be
classified)

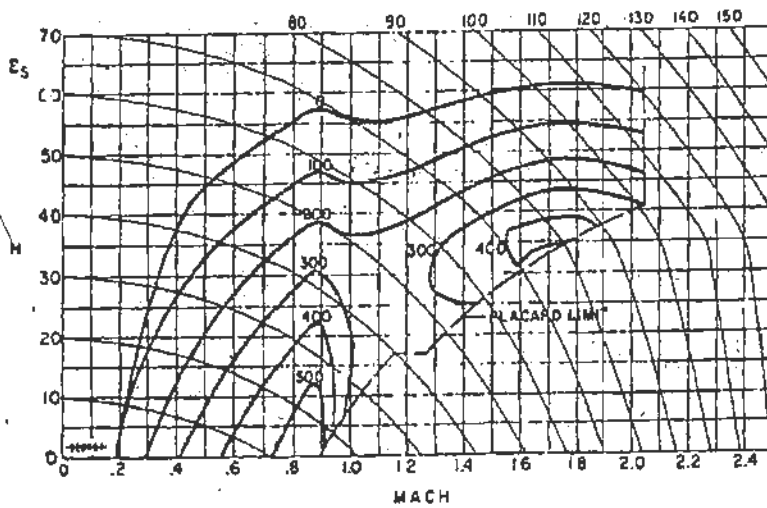


Figure 13. MIG-21 Maximum Power 1-C Energy Rate Diagram.

SECRET

SECRET

In Figures 14 through 17, we note that the F-4C retains most of its low-altitude subsonic/transonic sustained maneuvering advantage as g is increased from 1 to 5. In addition, these figures reveal that the MIG-21 not only has a supersonic advantage, but also is gaining regions of advantage subsonically since it can pull g in regions where the F-4C cannot operate. Essentially, such a condition indicates the MIG-21 can turn more quickly than, or inside, the F-4C. This same conclusion was reached by studying the $C-V$ diagram. Logically, this means the left-hand boundaries of the 1- g , 3- g , and 5- g Energy Rate diagrams provide a measure of instantaneous maneuverability, while entire diagrams provide a measure of sustained maneuverability as a function of energy rate and g .

(S) The military power 1- g Energy Rate diagrams (Figures 18 and 19) show that the F-4C has the ability to gain energy more rapidly than the MIG-21 throughout most of the envelope. The magnitude of this advantage is depicted in Table II.

TABLE II. RUTOWSKI MINIMUM TIME PATHS (MILITARY POWER)

Type Aircraft	$E_0 = 3,000$ ft to $E_1 = 45,000$ ft		
	Time (sec)	Fuel Weight Used (lb)	Fuel Used (%)
F-4C	309	1341	12
MIG-21	403	615	17

NASIC/ACAA
DECLASSIFY
(This information
no longer
needs to be
classified)

(S) By consulting the military power 3- g and 5- g Energy Rate diagrams (Figures 20 through 23), we observe that the F-4C has a sustained maneuvering advantage at the lower altitudes and higher Mac' numbers. These diagrams also reveal that the MIG-21 regions of advantage spread to the lower portion of the envelope as g is increased from 1 to 5. In addition, these diagrams (Figures 20 through 23) reveal that the MIG-21 can maneuver in regions unavailable to the F-4C. As mentioned previously, such a condition indicates that the MIG-21 can outturn the F-4C.

(S) From Figures 24 and 25, we observe that the F-4C has the subsonic advantage, while the MIG-21 has the supersonic advantage in terms of the maneuvering energy gained versus the percentage of internal energy expended. On the other hand, the variable fuel E-M Efficiency diagrams (Figures 26 and 27) reveal that the F-4C increases its subsonic advantage and acquires an advantage through most of the supersonic portion of the envelope. A natural question arises at this point as to why the F-4C appears to have a greater degree of advantage in the variable fuel diagram than in the

~~SECRET~~

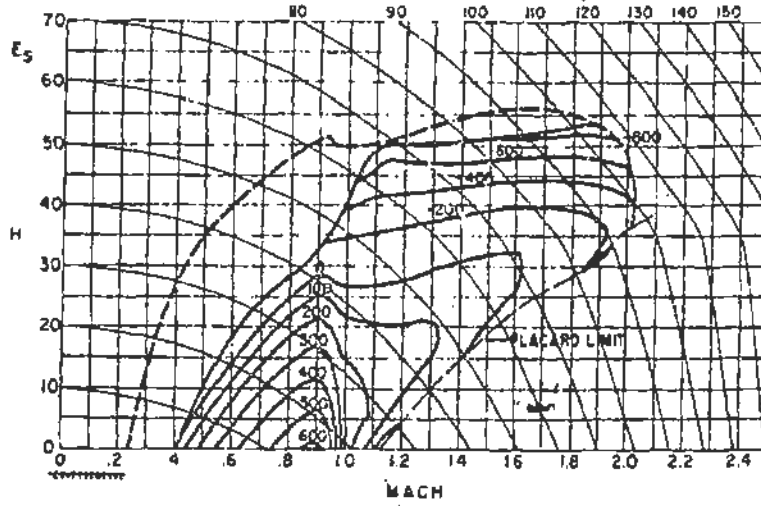


Figure 14. F-4C Maximum Power 3-G Energy Rate Diagram.

NASIC/ACAA
DECLASSIFY
(This information no
longer
needs to be classified)

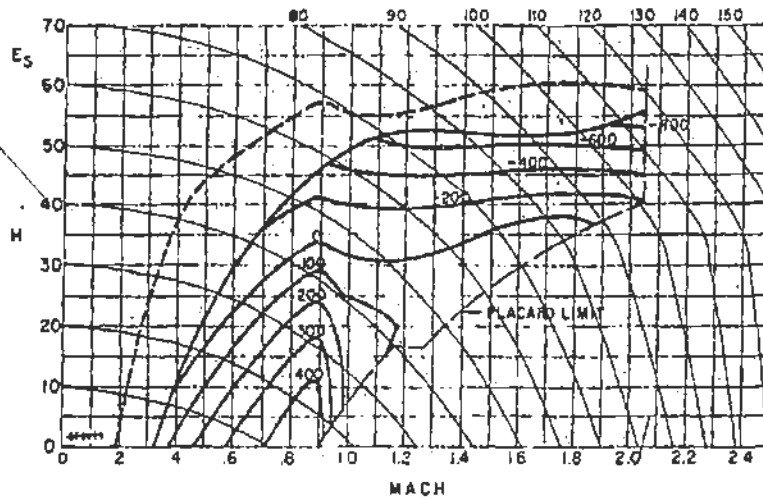


Figure 15. MiG-21 Maximum Power 3-G Energy Rate Diagram.

~~SECRET~~

~~SECRET~~

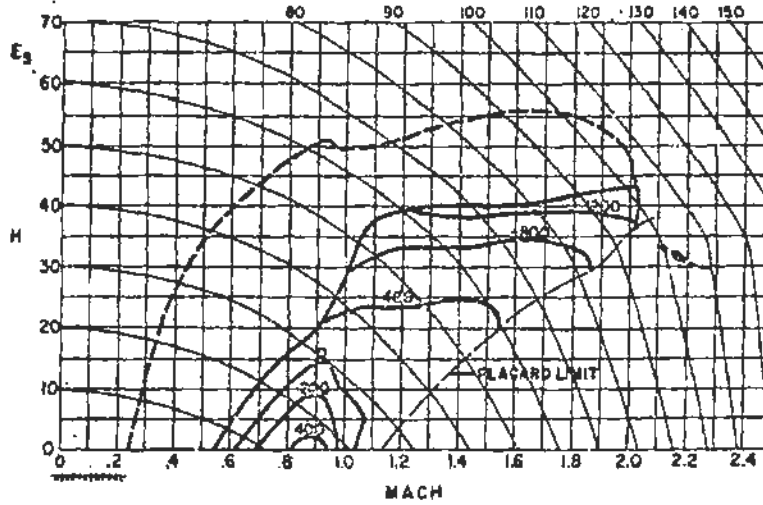


Figure 16. F-4C Maximum Power 5-G Energy Rate Diagram.

NASIC/ACAA
DECLASSIFY
(This information no
longer
needs to be
classified)

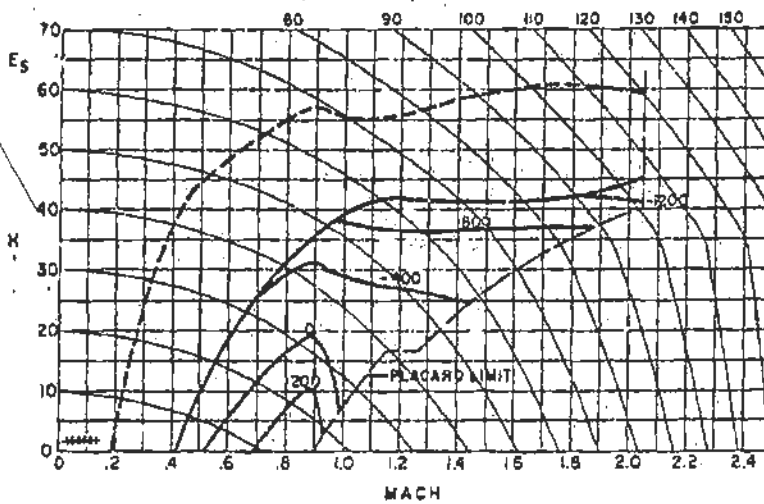


Figure 17. MIG-21 Maximum Power 5-G Energy Rate Diagram.

~~SECRET~~

SECRET

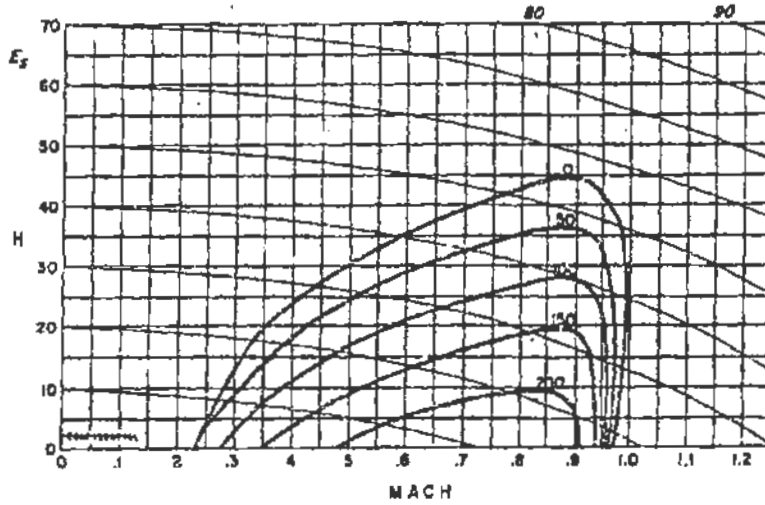


Figure 18. F-4C Military Power 1-G Energy Rate Diagram.

NASIC/ACAA
DECLASSIFY
(This information no
longer
needs to be classified)

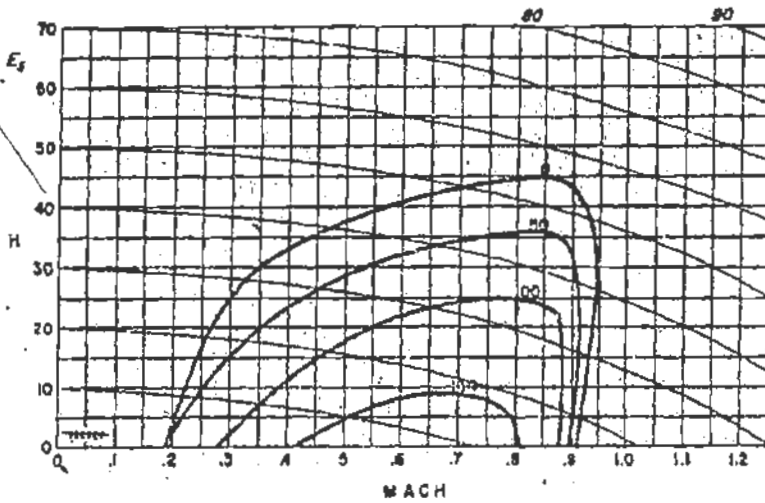


Figure 19. MIG-21 Military Power 1-G Energy Rate Diagram.

SECRET

SECRET

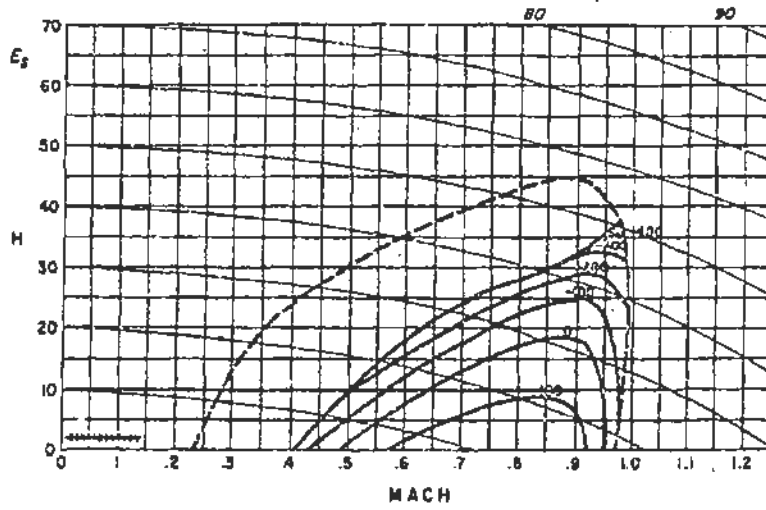


Figure 20. F-4C Military Power 3-G Energy Rate Diagram.

NASIC/ACAA
DECLASSIFY
(This information
no longer
needs to be
classified)

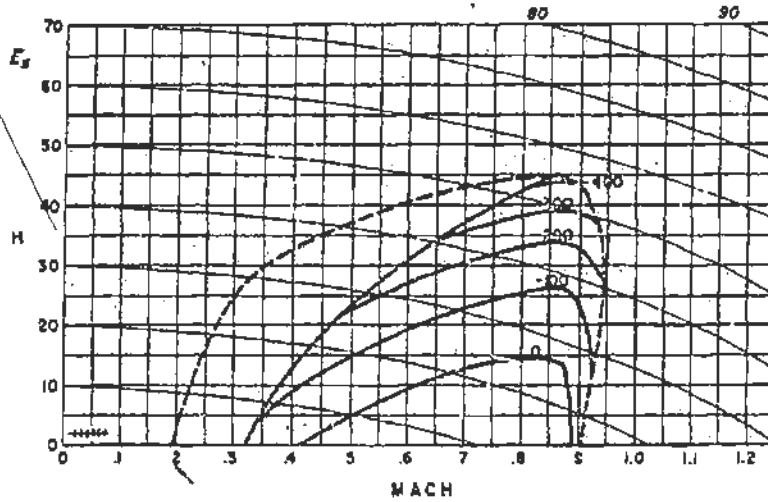


Figure 21. MIG-21 Military Power 3-G Energy Rate Diagram.

SECRET

~~SECRET~~

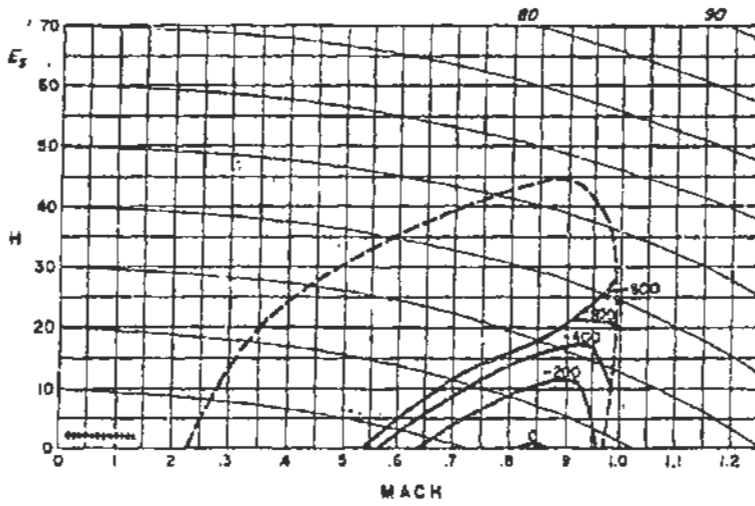


Figure 22. F-4C Military Power 5-G Energy Rate Diagram.

NASIC/ACAA
DECLASSIFY
(This information no
longer
needs to be
classified)

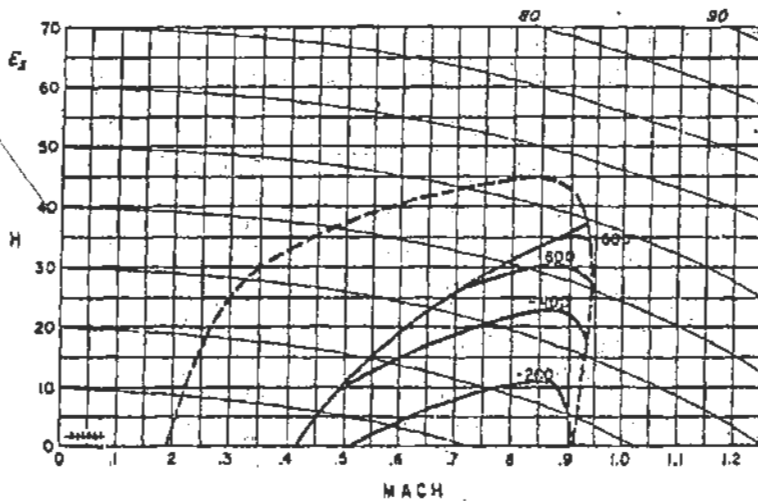


Figure 23. MIG-21 Military Power 5-G Energy Rate Diagram.

~~SECRET~~

~~SECRET~~

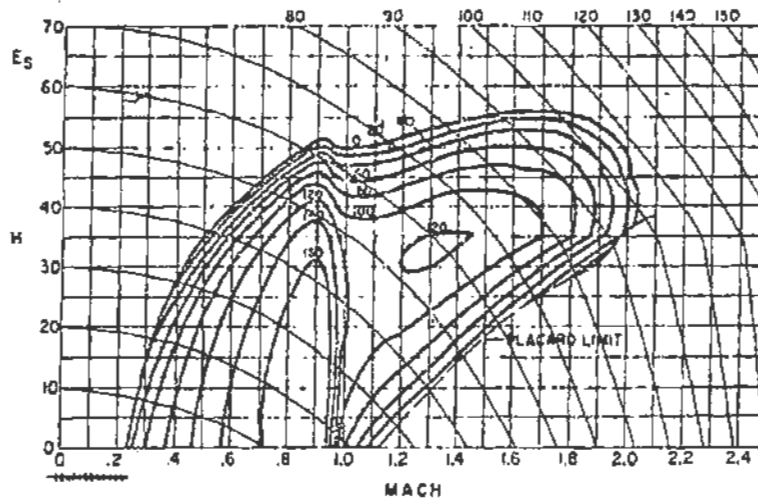


Figure 24. F-4C Maximum Power Constant (50%) Fuel E-M Efficiency Diagram.

NASIC/ACAA
DECLASSIFY
(This information no
longer
needs to be
classified)

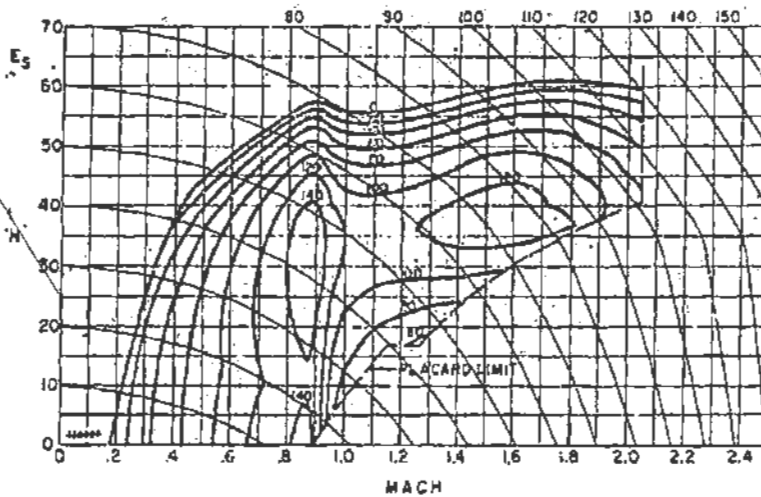


Figure 25. MIG-21 Maximum Power Constant (50%) Fuel E-M Efficiency Diagram.

~~SECRET~~

~~SECRET~~

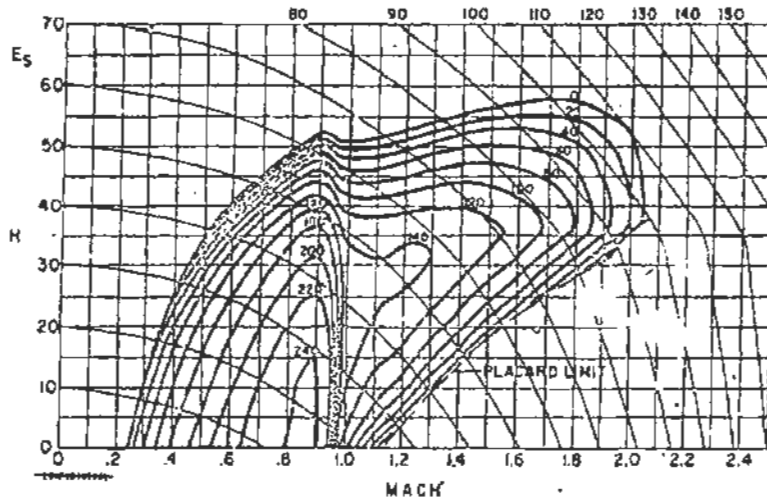


Figure 26. F-4C Maximum Power Variable Fuel E-M Efficiency Diagram.

NASIC/ACAA
DECLASSIFY
(This information no
longer
needs to be
classified)

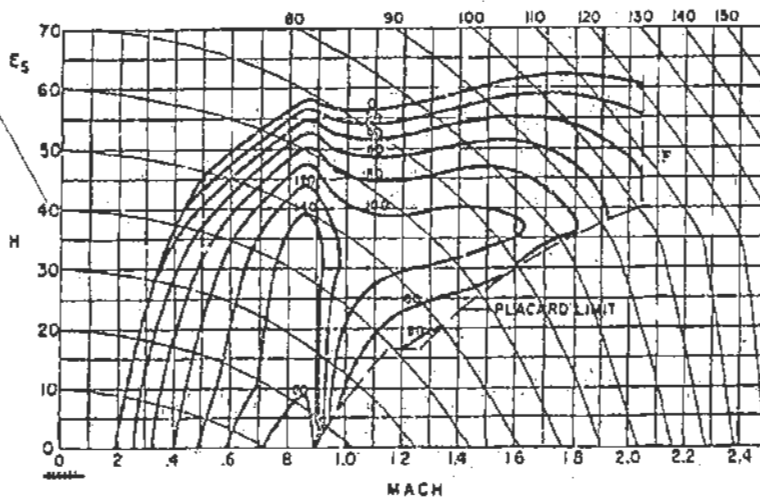


Figure 27. MiG-21 Maximum Power Variable Fuel E-M Efficiency Diagram.

~~SECRET~~

SECRET

constant fuel diagram. The greater advantage attributed to the F-4C in the variable fuel diagram results from the fact that the F-4C has expended a smaller percentage of its fuel when it reaches the regions where the MIG-21 is more efficient. Certainly such an advantage would not be realistic if the F-4C entered the engagement with a smaller percentage of fuel on board and/or the engagement started at a high subsonic energy level. If such a condition existed, the efficiency advantage attributed to the MIG-21 in the supersonic region of the constant fuel diagram would be realistic. This point of difference becomes important to the F-4C pilot when he encounters a MIG-21 in hostile territory. From the military power E-M Efficiency diagrams depicted in Figures 28 through 31, we see that the F-4C has the advantage in both cases, assuming, of course, that each aircraft has the same assumed or starting fuel percentages on board. Actual time and percentage values of fuel expended along minimum fuel paths between energy levels for these two aircraft are displayed in Tables III and IV.

TABLE III. RUTOWSKI MINIMUM FUEL PATHS (MAXIMUM POWER)

Type Aircraft	E ₁ = 3,000 ft to E ₂ = 70,000 ft			E ₁ = 3,000 ft to E ₂ = 95,000 ft		
	Time (sec)	Fuel Weight Used (lb)	Fuel Used (%)	Time (sec)	Fuel Weight Used (lb)	Fuel Used (%)
F-4C	252	3206	28	370	4970	44
MIG-21	223	1233	32	291	1713	44

TABLE IV. RUTOWSKI MINIMUM FUEL PATHS (MILITARY POWER)

Type Aircraft	E ₁ = 3,000 ft to E ₂ = 45,000 ft		
	Time (sec)	Fuel Weight Used (lb)	Fuel Used (%)
F-4C	325	1292	11
MIG-21	422	618	16

(S) The Range diagrams (Figures 32 and 33) reveal that the F-4C has a substantial advantage in the subsonic portion of the envelope and a lesser advantage in the supersonic portion of the envelope.

SECRET

NASIC/ACAA
DECLASSIFY
(This information
no longer
needs to be
classified)

SECRET

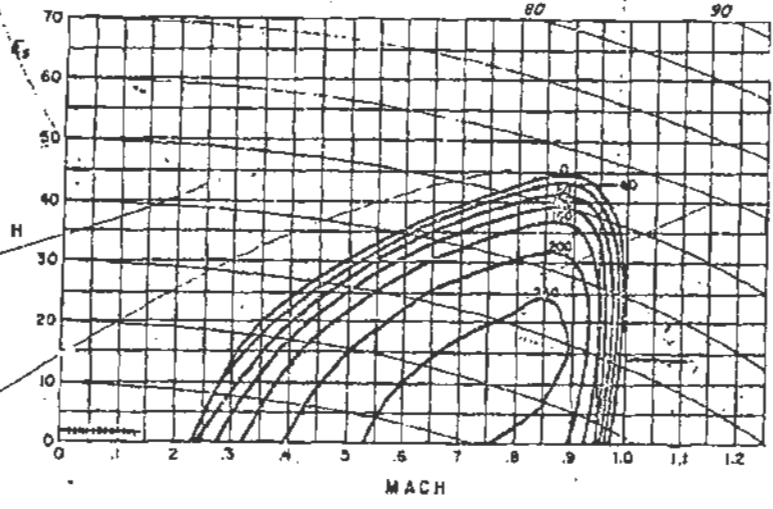


Figure 28. F-4C Military Power Constant (50%) Fuel E-M Efficiency Diagram.

NASIC/ACAA
DECLASSIFY
(This information
no longer
needs to be
classified)

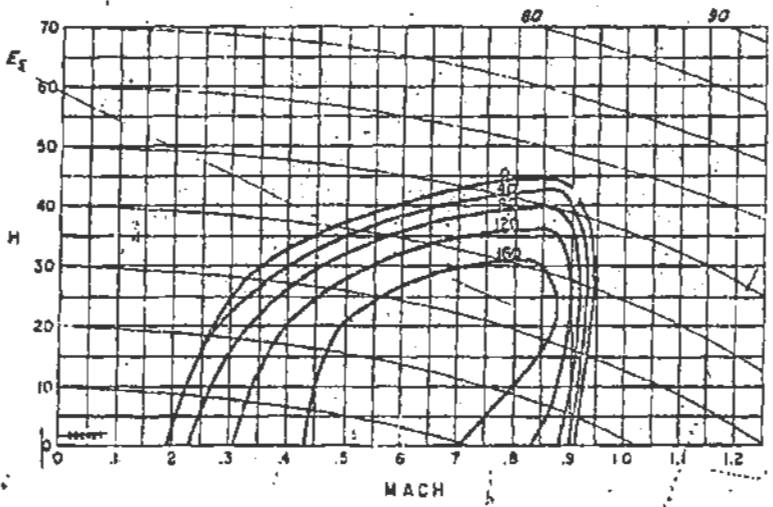


Figure 29. MiG-21 Military Power Constant (50%) Fuel E-M Efficiency Diagram.

SECRET

~~SECRET~~

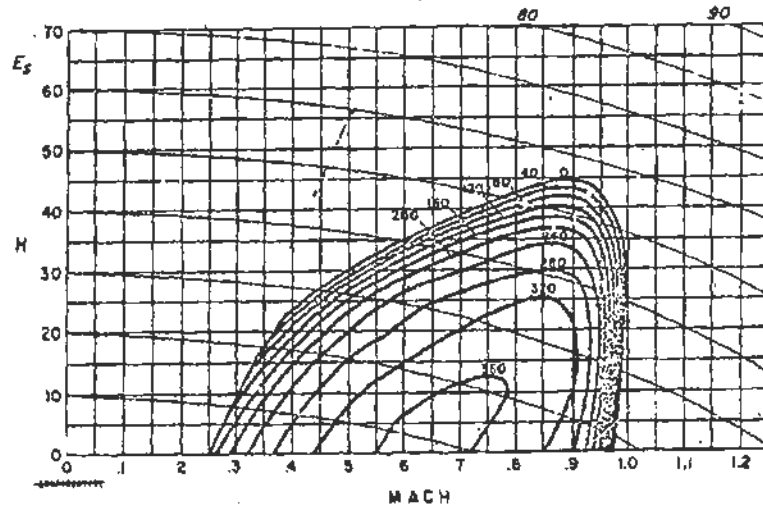


Figure 30. F-4C Military Power Variable Fuel E-M Efficiency Diagram.

NASIC/ACAA
DECLASSIFY
(This information
no longer
needs to be
classified)

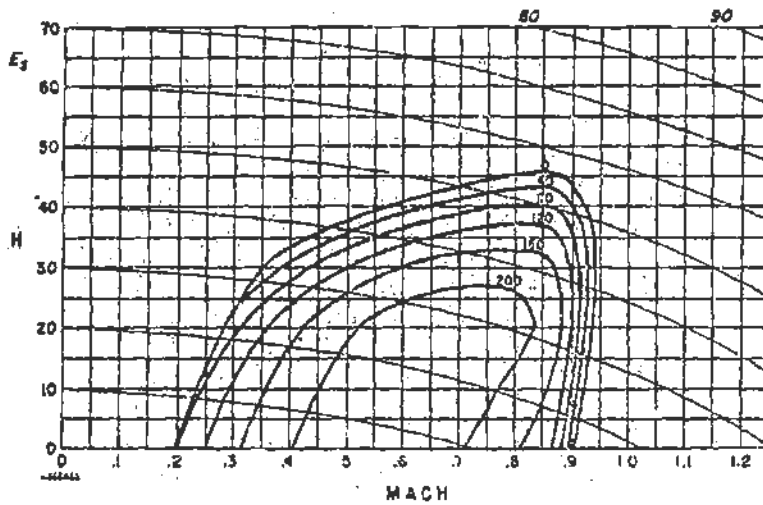


Figure 31. MIG-21 Military Power Variable Fuel E-M Efficiency Diagram.

~~SECRET~~

~~SECRET~~

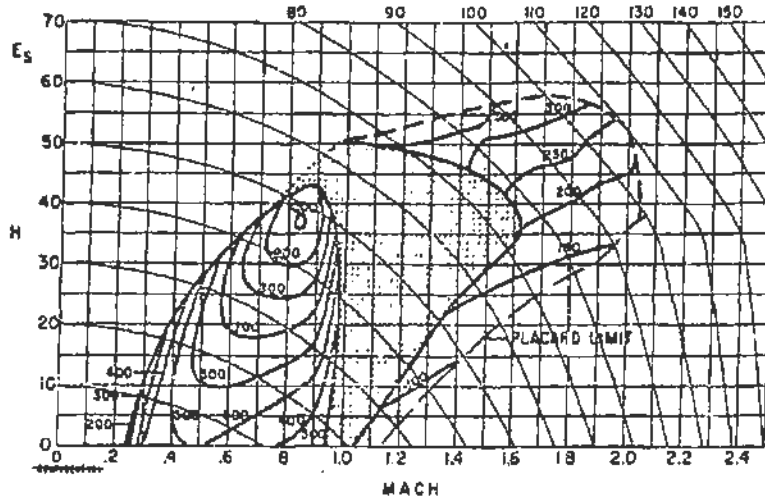


Figure 32. F-4C Range Diagram.

NASIC/ACAA
DECLASSIFY
(This information no
longer
needs to be
classified)

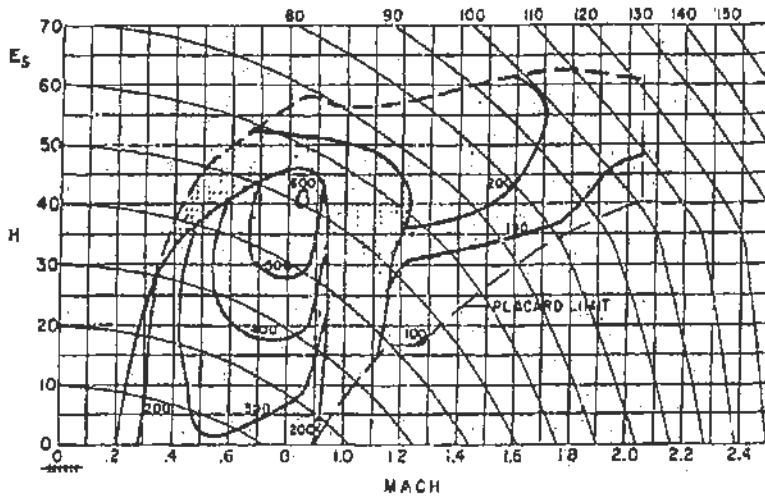


Figure 33. MIG-21 Range Diagram.

~~SECRET~~

SECRET

(7S) By comparing the rule-of-thumb performance of the AIM-9B/AA-2 and the AIM-7E (see Appendix I), we find the F-4C with four AIM-7E missiles has an enormous all-aspect, first-shot advantage over the MIG-21 equipped with internal gun(s) and two AA-2 missiles. This advantage prevails against either a maneuvering or nonmaneuvering MIG-21. However, in spite of this advantage, an F-4C pilot may find it difficult to employ AIM-7E during a re-attack or in an effort to nullify an attack, since the MIG-21 can easily outturn the F-4C as well as maintain more energy while doing so. By exploiting this dual advantage, a skillful MIG-21 pilot may prevent a successful AIM-7E missile launch by simply maneuvering away from the front toward the rear hemisphere of the F-4C. For close-in maneuvering, the F-4C can mount a 20 millimeter centerline gun pod in addition to the four AIM-7 missiles in an effort to get inside the missile minimum firing range restrictions. However, such a fix results in an even greater margin of maneuvering superiority for the MIG-21 by reducing the already inferior instantaneous and sustained maneuverability of the F-4C. The magnitude of this maneuverability loss for the F-4C can be determined by consulting the energy diagrams in Volume III of this report, to be published at a later date.

(8) From the foregoing analysis, it is clear that the MIG-21 enjoys an enormous instantaneous maneuvering advantage and a substantial sustained maneuvering advantage in terms of energy rate and g throughout the supersonic portion of the flight envelope. Subsonically, at both maximum and military power, the MIG-21 has a sustained maneuvering advantage in the upper portions of the envelope that spread to the lower portions as g increases. On the other hand, the F-4C has a sustained maneuvering advantage in terms of efficiency throughout the entire subsonic portion of the envelope extending through most of the supersonic envelope. Only in range and first-shot capability does the F-4C enjoy a substantial advantage over the MIG-21.

(U) Naturally, for a complete analysis, additional information must be developed. The tactician needs energy-maneuverability diagrams for various type combat configurations. In addition, he needs comparative missile firing envelopes together with radar and maneuvering constraints that may be imposed on the pilot or radar operator. If this information is provided, the tactician can design tactics by using energy-maneuverability methods. Assuming that Foreign Technology Divisions can provide reasonably accurate data concerning enemy performance, the tactician, for the first time, can develop effective tactics against any adversary. In addition, tactical commanders can use the energy-maneuverability comparative analyses to gain meaningful perspective for decisions concerning the employment of friendly fighters against a known enemy.

~~CONFIDENTIAL~~

SECTION V

REQUIREMENTS

(U) Presently, in order to meet mission requirements, Air Force planners direct that new designs meet certain specifications in terms of altitude, air-speed, acceleration, g, and range. Contractors, in an effort to satisfy the customer, produce designs to meet these specifications. However, no guarantee can be made that the design selected will be the best one since such specifications are point data (derivatives) and provide no indication of an aircraft's integrated performance and design efficiency throughout the flight envelope.

(U) However, by applying energy-maneuverability techniques, along with other information deemed necessary by the tactician, planners would have the advantage of looking at complete performance (including the previously mentioned point data) before making decisions concerning aircraft requirements. As a result, true operational need would be considered by both planners and designers in determining the best overall combination of armament, engine, and airframe in future designs.

~~CONFIDENTIAL~~

(This page is unclassified.)

~~CONFIDENTIAL~~

88th ABW/IPI
FOIA (b)(1)(3)
E.O. 13526
Sec 3.3 (b)(4) (a)(g)

APPENDIX I

RULE-OF-THUMB PERFORMANCE CAPABILITY OF AIM-7E AND AIM-9B/AA-2 MISSILES

Withheld from public release
under statutory authority
of the Department of Defense
FOIA 5 USC §552(b)(3)
10 USC § 130

(S) The Air Force Armament Laboratory (AFATL), Research and Technology Division, AFSC, Eglin Air Force Base, Florida, AIM-9B six-degree-of-freedom, digital computer program was employed to produce over one hundred launch envelopes. E.O. 13526, section 3.3(b)(4)

The Raytheon Company, Bedford, Massachusetts, by means of an analog computer, produced launch envelopes and a parametric study of AIM-7E missiles against targets also pulling from 1 g to 5 g (see Reference 7). A spot check by AFATL's AIM-7E five-degree-of-freedom, digital computer program showed excellent agreement with the Raytheon Company results. An analysis of the AIM-7E and AIM-9B/AA-2 launch envelopes revealed the rule-of-thumb performance presented in this appendix for these missiles. Typical launch envelopes used to develop the rule-of-thumb performance are shown in Figures I-1 and I-2.

(S) By carefully noting trends or patterns, the rule-of-thumb performance of the AIM-7E and AIM-9B/AA-2 missiles can be further simplified by tactical organizations for operational use.

AIM-7E MISSILES

(S) MINIMUM RANGE. Minimum range (R_{min}) for nose quarter (NQ), beam (AB), and tail quarter (TQ) attacks:

Altitude (ft)	Type of Attack		
	NQ (ft)	AB (ft)	TQ (ft)
SL	8,500	7,600	5,100
10,000	9,250	8,100	5,400
20,000	10,100	8,600	5,800
30,000	11,400	9,200	6,300
40,000	12,800	9,800	6,800

For turns into the attack, add 1,000 ft to the above values. For turns away from the attack, subtract 1,000 ft.

~~CONFIDENTIAL~~

80th ABW/IPI
FOIA (b)(1)(b)(3) 10 USC. 130
E.O. 13526
Sec 3.3 (b)(4) 1.4. (a)(g)

~~CONFIDENTIAL~~

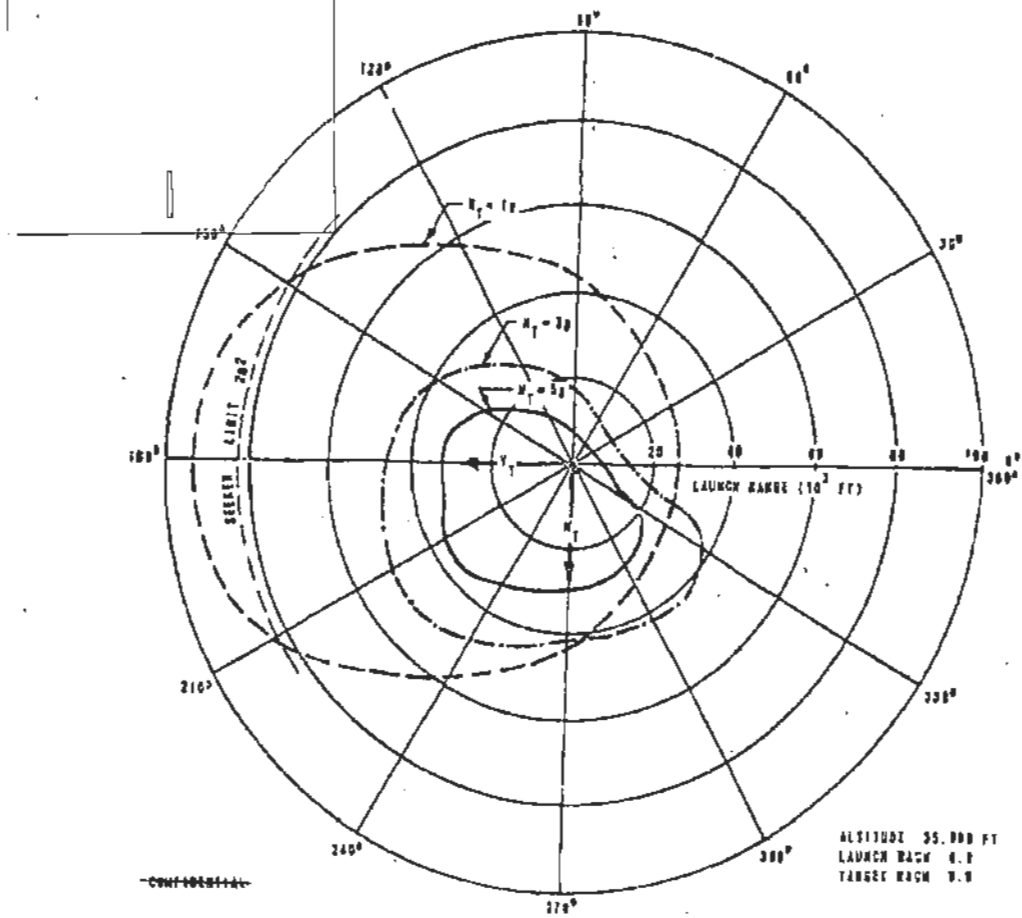
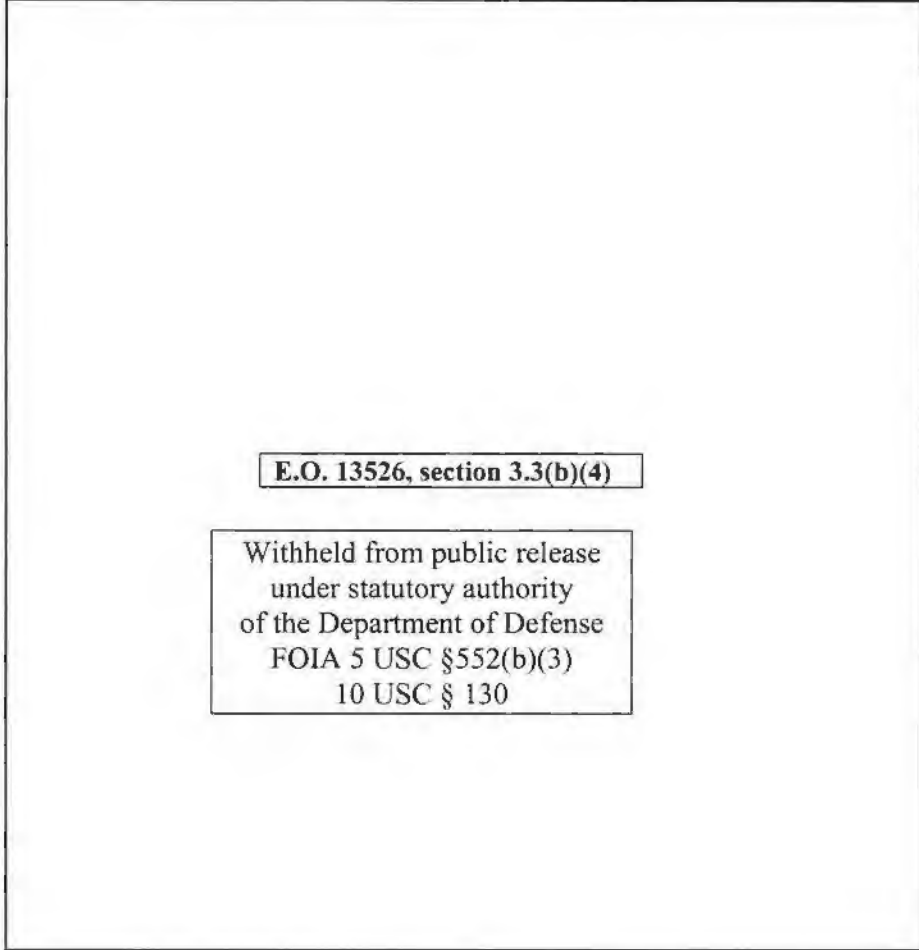


Figure I-1. AIM-7E Missile Launch Envelope

~~CONFIDENTIAL~~

88th ABW/IPI
FOIA (b)(1)(b)(3) 10 USC
130
E.O. 13526
Sec 3.3 (b)(4) 1.4. (a)(g)

~~CONFIDENTIAL~~



E.O. 13526, section 3.3(b)(4)

Withheld from public release
under statutory authority
of the Department of Defense
FOIA 5 USC §552(b)(3)
10 USC § 130

Figure 1-2. AIM-9B/AA-2 Missile Launch Envelope

~~CONFIDENTIAL~~

~~CONFIDENTIAL~~

(S) MAXIMUM RANGE. Against a Co-Speed Nonmaneuvering Target. Maximum range (R_{max}) and angle-off (ϕ_{max}) for a nose quarter, abeam, and tail quarter attack against a co-speed nonmaneuvering target:

Subsonic Target - Mach 0.9:

Altitude (ft)	NQ/ ϕ (ft/deg)	AB (ft)	TQ/ ϕ (ft/deg)
SL	80,000/10	15,000	9,000/30
10,000	82,000/10	22,000	13,000/30
20,000	82,000/12	30,000	19,000/30
30,000	82,000/25	40,000	26,000/30
40,000	82,000/40	52,000	35,000/30

For a subsonic target Mach 0.5 at sea level, NQ/ $\phi = 60,000$ ft/10°, AB = 24,000 ft, and TQ/ $\phi = 18,000$ ft/30°. For each additional 10,000 ft, add 5,000 ft to NQ, 8,000 ft to AB, and 5,000 ft to TQ.

Supersonic Target:

Altitude (ft)	NQ/ ϕ (ft/deg)	AB (ft)	TQ/ ϕ (ft/deg)
SL	82,000/10	--	--
10,000	82,000/10	12,000	7,000/30
20,000	82,000/15	20,000	14,000/30
30,000	82,000/30	30,000	20,000/30
40,000	82,000/45	40,000	28,000/30

(S) Against Nonmaneuvering Targets with Attacker Velocity Greater or Less than Target Velocity. Maximum ranges for nose quarter and tail quarter attacks against nonmaneuvering targets with attacker velocity greater or less than target velocity (Δ Mach) follow:

Nose Quarter Attacks:

1. Add 3,000 feet to R_{max} for each 0.1 Δ Mach below 10,000 feet when target velocity is greater than attacker velocity.
2. Add 1,500 feet to R_{max} for each 0.1 Δ Mach above 10,000 feet when target velocity is greater than attacker velocity.
3. Add 1,000 feet to R_{max} for each 0.1 Δ Mach when attacker velocity is greater than target velocity.

~~CONFIDENTIAL~~

~~CONFIDENTIAL~~

Tail Quarter Attacks:

1. Add 2,000 feet to R_{max} for each 0.1 delta mach rate of closure.
2. Subtract 3,000 feet from R_{max} for each 0.1 delta mach separation.

~~(S)~~ Against a Maneuvering Target.

Nose Quarter Attacks:

1. Reduce R_{max} 30,000 feet when target maneuvers away from the attack at 2 g.
2. Reduce R_{max} 5,000 feet/g for target maneuvers away from the attack with g greater than 2.

~~(S)~~ Maneuvers Away from Attack, Tail Quarter Attacks.

Altitude	Target G	$R_{(max)}$
Below 20,000 ft	3	$2/3 R_{max}$
Below 20,000 ft	5	$1/2 R_{max}$
Above 20,000 ft	3	$1/2 R_{max}$
Above 20,000 ft	5	$1/3 R_{max}$

The above values do not include background clutter associated with a target at low altitude.

E.O. 13526, section 3.3(b)(4)

Withheld from public release
under statutory authority
of the Department of Defense
FOIA 5 USC §552(b)(3)
10 USC § 130

~~CONFIDENTIAL~~

88th ABW/IPI
FOIA (b)(1)(b)(3)10
USC 130
E.O. 13526
Sec 3.3 (b)(4) 1.4 (a)(g)

~~CONFIDENTIAL~~

E.O. 13526, section 3.3(b)(4)

Withheld from public release
under statutory authority
of the Department of Defense
FOIA 5 USC §552(b)(3)
10 USC § 130

~~CONFIDENTIAL~~

88th ABW/IPI
FOIA (b)(1)(b)(3)10 USC
130
E.O.13526
Sec 3.3 (b)(4), 1.4. (a)(g)

~~CONFIDENTIAL~~

E.O. 13526, section 3.3(b)(4)

Withheld from public release
under statutory authority
of the Department of Defense
FOIA 5 USC §552(b)(3)
10 USC § 130

~~CONFIDENTIAL~~

APPENDIX II

MATHEMATICAL DERIVATIONS AND MODELS FOR DEVELOPING ENERGY-MANEUVRABILITY THEORY AND ASSOCIATED FLIGHT PATHS

(Appendix II is unclassified in its entirety)

In this appendix a discussion of the mathematical methods employed to develop the Energy-Maneuverability Theory and associated flight paths in the altitude-Mach number plane will be presented. For convenience, the derivations will be described in terms of the following computer programs which have been formulated to handle the computational aspects of the theory:

- Part I - Basic Energy-Maneuverability Computer Model
- Part II - The Bryson-Kelley Steepest Ascent Optimization Program
- Part III - Dynamic Profile Generator Program

PART I. BASIC ENERGY-MANEUVRABILITY COMPUTER MODEL

DERIVATIONS

INSTANTANEOUS MANEUVERABILITY. For any given aircraft, maximum load factor (normal acceleration) may be computed as a function of altitude and airspeed:

$$n_L = \frac{q S C_{L_{max}}}{W}$$

where n_L = maximum normal acceleration (dimensionless)

$q = \frac{1}{2} \rho V^2$, dynamic pressure (lb/ft²)

ρ = atmospheric density (slugs/ft³)

V = true airspeed (ft/sec)

S = reference wing area (ft²)

$C_{L_{max}}$ = maximum coefficient of lift (dimensionless)

W = aircraft weight (lb)

Since calibrated airspeed (CAS) is more meaningful to the pilot than true airspeed, the G-V diagrams (see Figure 1, page 3) depict maximum normal acceleration versus CAS.

SUSTAINED MANEUVERABILITY. Energy Rate. The energy (E) possessed by an aircraft is the sum of its potential energy (E_p) and its kinetic energy (E_k). Mathematically,

$$\begin{aligned} E &= E_p + E_k \\ &= wh + \frac{1}{2} mV^2 \\ &= w \left(h + \frac{V^2}{2g} \right), \end{aligned}$$

where

h = altitude (ft)

m = aircraft mass (slugs)

$g = 32.174$ ft/sec², the gravitational acceleration

The expression, $E = w \left(h + \frac{V^2}{2g} \right)$, gives us a measure of the energy state of an aircraft at any altitude-airspeed combination. However, since the main interest lies in comparing aircraft with different weights at the same altitude-airspeed combinations, it is more meaningful to make the above expression independent of aircraft weight. Dividing both sides of the above expression by w yields

$$\frac{E}{w} = h + \frac{V^2}{2g} .$$

The term E/w can be regarded as specific energy (E_s), with the result that the energy state of an aircraft can now be expressed as a function of altitude and airspeed:

$$E_s = h + \frac{V^2}{2g} .$$

The problem of managing energy involves controlling the rate of transfer between energy levels. Differentiating the above expression results in

$$\dot{E}_s = \dot{h} + \frac{V\dot{V}}{g} ,$$

where the dot ($\dot{}$) indicates the derivative with respect to time, $\frac{d}{dt}$. To provide more insight into energy rate, \dot{E}_s , we may employ Figure II-1 and write a force balance equation along the flight path.

$$m\dot{V} = T_s - D - w \sin \gamma ,$$

or

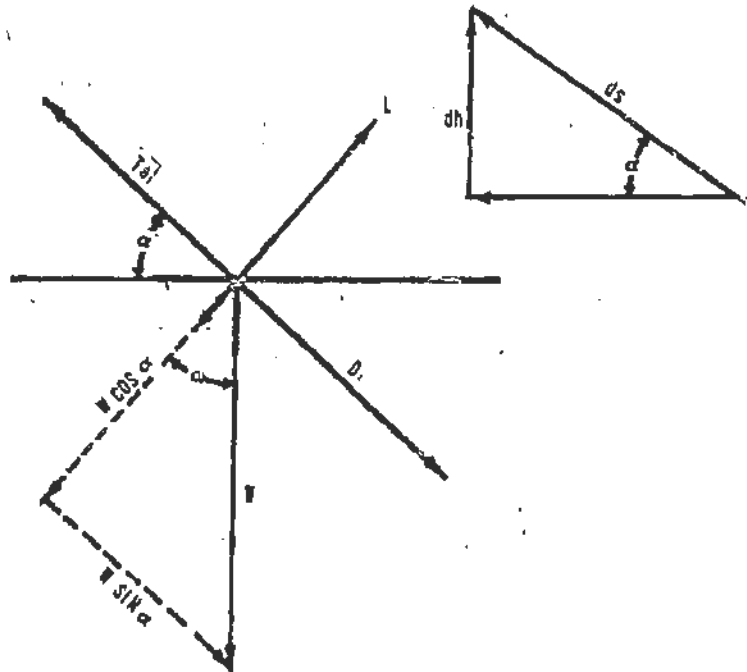
$$T_s - D = w \sin \gamma + \frac{w}{g} \dot{V} ,$$

or

$$\frac{T_s - D}{w} = \sin \gamma + \frac{\dot{V}}{g} .$$

Multiplying both sides of this expression by V yields

$$\left(\frac{T_s - D}{w} \right) V = V \sin \gamma + \frac{V\dot{V}}{g} .$$



UNCLASSIFIED

Figure II-1. Aircraft Force-Balance Diagram.

Since $\dot{h} = V \sin \gamma$, we may write

$$\left(\frac{T_a - D}{W}\right) V = \dot{h} + \frac{V\dot{V}}{g}$$

The right side of the above expression is equal to \dot{E}_s . Recalling that work is accomplished in transferring from one energy level to another, and that power, by definition, is the time rate of doing work, the left side of the above equation may be equated to specific excess power, P_s :

$$P_s = \dot{E}_s = \left(\frac{T_a - D}{W}\right) V.$$

In an attempt to counter an immediate threat, the energy-oriented fighter pilot will strive to increase his maneuvering energy as quickly as possible. This amounts to maximizing the rate of transfer between energy levels, which is equivalent to maximizing the integral

$$E_s = \int_{t_1}^{t_2} P_s dt.$$

According to Rutowski (reference 1), this is accomplished when

$$\left[\frac{\partial P_s}{\partial V}\right]_{E_s=k} = 0,$$

or

$$\left[\frac{\partial E_s}{\partial h}\right]_{E_s=k} = 0.$$

In the altitude-Mach number plane, these relationships are satisfied at those points where the E_s contours are tangent to the $L-g P_s$ contours. Connecting these points results in an approximate minimum time path.

Energy-Maneuverability Efficiency (E-ME). If the above-mentioned threat is not as imminent, the pilot will attempt to increase his maneuvering energy while conserving internal energy (fuel) for future maneuverability. This is achieved by maximizing the integral

$$E_s = \int_{w_1}^{w_2} \frac{dE_s}{dw} dw.$$

Since $dE_s = P_s dt$,

and $dw = -\dot{w}_f dt$ (\dot{w}_f = fuel flow - lb/sec)

we see that

$$\frac{dE_s}{dw} = -\frac{P_s}{\dot{w}_f}$$

and

$$E_s = - \int_{w_1}^{w_2} \frac{P_s}{\dot{w}_f} dw$$

Again, by employing Rutowski's technique, we obtain

$$\left(\frac{\partial(P_s/\dot{w}_f)}{\partial V} \right)_{E_s=k} = 0,$$

or

$$\left(\frac{\partial(P_s/\dot{w}_f)}{\partial h} \right)_{E_s=k} = 0,$$

These relationships are satisfied at those points in the altitude-Mach number plane where the E_s contours are tangent to the 1-g P_s/\dot{w}_f contours. Connecting these points results in an approximate minimum fuel path.

The P_s/\dot{w}_f contours suggest a measure of efficiency in view of the fact that they depict the amount of specific energy gained per pound of fuel expended. In order to acquire a more meaningful measure of efficiency, these contours can be modified to portray the amount of maneuvering energy gained for the internal energy (fuel) expended. This is done by multiplying the P_s/\dot{w}_f contours by the weight of fuel available, w_{fa} , to obtain the resulting expression for Energy-Maneuverability Efficiency:

$$E-ME = \frac{P_s^*}{\dot{w}_f} w_{fa}$$

where P_s^* = the average P_s over the fuel weight interval w_{fa} - $fc \leq w_f \leq w_{fr}$ (ft/sec), and $w_{fa} = w_{r0} - fc - w_{fr}$

where w_{r0} = initial fuel weight (lb)

fc = fuel consumed in flying from some reference energy level to any given altitude-Mach number point (lb)

w_{fr} = fuel reserve (lb)

RANGE. For any altitude-airspeed combination, available range for cruise condition may be expressed as

$$R = \frac{W_0^*}{W_0} V + x,$$

where W_0^* = the average cruise fuel flow, W_0 , over the fuel weight interval

$$W_0 - \Delta W \leq W \leq W_0, \text{ (lb/sec),}$$

and x = the horizontal distance traversed in flying from some reference energy level to any given altitude-airspeed combination.

COMPUTATIONS

ENERGY RATE DIAGRAMS. For any given aircraft, an Energy Rate diagram may be constructed by dividing the altitude-Mach number plane into a rectangular grid, computing energy rate (P_e) values at all of the points of intersection of the grid lines, and then connecting points of equal P_e . The contour defined by $P_e = 0$ represents the steady-state boundary of the aircraft. An aircraft cannot operate outside this contour without losing energy, either in the form of altitude, airspeed, or some combination of both. The steady-state boundary is further restricted on the left by the buffet boundary (obtained by connecting points where $C_L = C_{L_{max}}$), and on the right by placard limits (a combination of pressure [structural] limits and engine temperature limits).

Considerable insight into the effects of pulling g within the aircraft's flight envelope can be gained by constructing Energy Rate diagrams of more than $1g$. These diagrams contain both positive and negative P_e contours within the $1-g$ steady-state envelope. As such, they provide a measure of sustained maneuverability as a result of pulling g within the envelope.

E-M EFFICIENCY DIAGRAMS. Computational aspects of this diagram proceed in the same manner as for the Energy Rate diagrams, except that now we compute and connect points of equal E-ME. Two different types of E-ME diagrams are constructed. The first type is referred to as the path independent (constant fuel) E-ME diagram. Computations for all points in the envelope are based on 50% fuel weight. Since fuel weight is held constant, the expression

$$E-ME = \frac{P_e}{W_0} W_0,$$

reduces to

$$E-ME = \frac{P_s}{W_f} W_{T_s}$$

The diagram is called path-independent since the amount of fuel at the altitude-Mach number points where computations are made is independent of the paths required to reach these points.

In the second type of E-ME diagram, called the path-dependent (variable fuel) E-ME diagram, the amount of fuel required to reach any given altitude-Mach number point is subtracted from the total fuel weight before E-ME computations are made. The assumption is that the pilot has flown a minimum fuel path from some reference energy level (we use $E_{REF} = 3000$ feet) to the altitude-Mach number point under consideration. A more detailed discussion of this assumption will be given later in this appendix and in Appendix III. Additionally, the amount of fuel upon which the path-dependent E-ME computations are based is reduced by a suitable reserve (normally 5% of full internal plus 20 minutes loiter at 10,000 ft).

RANGE DIAGRAMS. Again, the computational aspects of this diagram are essentially the same as for the Energy Rate and E-M Efficiency diagrams. To compute range, the program requires, as an additional input, a partial power setting table, i.e., a table of cruise fuel flow as a function of altitude, Mach number, and drag (thrust required). The subsonic and supersonic portions of the envelope are computed using partial military and partial afterburner power settings, respectively. A transient region is observed between the subsonic and supersonic portions of the envelope. In this region, level unaccelerated flight is not possible as the thrust required is greater than military thrust available, yet less than minimum afterburner thrust available.

For range, only a path-dependent (variable fuel) Range diagram is constructed. For this diagram, the amount of fuel available at any given altitude-Mach number point is reduced by the amount of fuel required to fly a minimum fuel path from some reference energy level (again, we use $E_{REF} = 3000$ feet) to the point under consideration, and by a suitable fuel reserve (c.g., 5% of full internal plus 20 minutes loiter at 10,000 feet). The horizontal distance traversed in flying the above-mentioned minimum fuel path, x , is considered part of the available range. A discussion of the method used to compute fuel consumed and horizontal distance traversed is given later in this appendix and in Appendix III.

EXTENSIONS OF THE RUTOWSKI TECHNIQUE

Earlier in this appendix, we saw that Rutowski calculated the location of the approximate minimum time and minimum fuel paths in the altitude-Mach number plane. Rutowski did not, however, give any measure of the time required, fuel consumed, or horizontal distance traversed in flying along these approximate paths. His two basic assumptions were that (1) the path be computed for 1 g and (2) the weight be held constant.

Rutowski's method has been extended to allow an approximation of the time required, fuel consumed, and horizontal distance traversed in flying along the minimum time or minimum fuel path. A byproduct of this extension has been the removal of his constant weight assumption.

Computations proceed as follows. Program inputs include initial, incremental, and final values for E_s and h :

$$E_{s,1} (\Delta E_s) E_{s,L}$$

$$h_1 (\Delta h) h_L$$

The specific energy equation,

$$E_s = h + \frac{V^2}{2g}$$

is rearranged to the form

$$V = [2g (E_s - h)]^{1/2}$$

Then for $E_s = E_{s,1}, E_{s,1} + \Delta E_s, E_{s,1} + 2\Delta E_s, \dots, E_{s,L}$, the following array is constructed:

h_1	V_1	M_1	$T_{a,1}$	\dot{w}_1	$C_{L,1}$	$C_{D,1}$	D_1	$P_{s,1}$	$(P_s/\dot{w}_1)_1$
h_2	V_2	M_2	$T_{a,2}$	\dot{w}_2	$C_{L,2}$	$C_{D,2}$	D_2	$P_{s,2}$	$(P_s/\dot{w}_1)_2$
.
.
.
h_L	V_L	M_L	$T_{a,L}$	\dot{w}_L	$C_{L,L}$	$C_{D,L}$	D_L	$P_{s,L}$	$(P_s/\dot{w}_1)_L$

Actually the array does not run all the way from h_1 to h_L . The lower altitudes result in Mach numbers higher than the aircraft's capability. When this occurs, altitude is incremented instead of computing T_a , \dot{W} , ..., P_s/\dot{W} . The higher altitudes result in C_L 's greater than $C_{L_{max}}$. This fact eliminates many of the lower lines of the array. Additionally, when $h > E_s$, the quantity $[2g(E_s - h)]^{\frac{1}{2}}$ becomes negative, eliminating lines of the array. Finally, other numerical techniques, beyond the scope of this appendix, are employed to reduce the size of the above arrays, thereby decreasing the computer time required to construct a path.

If a minimum time path is being computed, the program selects the altitude-Mach number point for which P_s is maximum in the array and this point becomes a point on the minimum time path. Once the line containing the maximum P_s is selected, it is used, along with a similar line on the previous array, to approximate a time increment, Δt , a fuel increment, ΔW , and a horizontal distance increment, Δx , in the following manner:

$$\Delta t = \frac{\Delta E_s}{\bar{P}_s} \quad \left(\text{the bar denotes the average, e.g., } \bar{P}_s = \frac{P_{s,i} + P_{s,i-1}}{2} \right)$$

$$\Delta W = \frac{\Delta E_s}{(P_s/\dot{W})}$$

$$\Delta x = \left[\bar{V}^2 - \left(\frac{\Delta h}{\Delta t} \right)^2 \right]^{\frac{1}{2}} \Delta t$$

The method outlined above results in altitude-Mach number points through which a minimum time path may be drawn. The Δt 's, ΔW 's, and Δx 's are summed over the path to give an approximation of the time required, fuel consumed, and horizontal distance traversed.

Each time E_s is incremented, the weight used to compute the quantities in the array is first decremented by the quantity ΔW , computed in the previous array. This results in a variable weight path.

Computations for a minimum fuel path proceed in exactly the same manner, except that, for the minimum fuel path, the line is chosen in the arrays where P_s/\dot{W} instead of P_s , is maximum.

To compute a path-dependent E-ME or Range diagram, a Rutowski minimum fuel path must be computed first and the following table built:

$E_{s,1}$	fc_1	x_1
$E_{s,2}$	fc_2	x_2
.	.	.
.	.	.
.	.	.
$E_{s,i}$	fc_i	x_i
.	.	.
.	.	.
$E_{s,L}$	fc_L	x_L

where

$$fc_i = \sum_{j=1}^i \Delta W_j,$$

and

$$x_i = \sum_{j=1}^i \Delta x_j.$$

Then, when L-ME or range is computed for a given altitude-Mach number point, (h, M), that (h, M) determines an E_s , which, in turn, determines an fc and an x , if we assume that the fuel consumed and horizontal distance traversed in flying to any point on a constant specific energy line is the same. This is a rather bold assumption, however, and cannot be accepted without further discussion. Appendix III provides a detailed treatment of this assumption.

PART II. THE BRYSON-KELLEY STEEPEST ASCENT OPTIMIZATION PROGRAM

The second computer program employed in these analyses is the Bryson-Kelley Steepest Ascent Optimization Program which provides dynamic flight profiles, in minimum time or with minimum expenditure of fuel, for transfer between two energy levels (h_1, M_1) and (h_2, M_2) .

By using the methods of E.S. Rutowski, the so-called Rutowski path, explained previously under the Energy-Maneuverability Program, is obtained and is depicted in Figure 3, page 7 of this report. However, these methods provide nothing more than very good approximations to the solution of the minimum time or minimum fuel problems. They provide no insight into such parameters as load factor or pitch angle along the path. In addition, the methods are predicated on 1-g level flight parameters and do not consider the forces acting perpendicular to the flight path. In essence, the Rutowski method is a static method, in itself, but a very valuable tool leading to the more accurate dynamic optimum paths.

Even the more sophisticated Dynamic Profile Generator Program, discussed in Part III of this Appendix, provides only approximations to the desired solution to the minimum time or fuel problem. Admittedly, the results of using the Rutowski paths in conjunction with this program are much more realistic, as now both load factor and pitch angle are considered throughout the path. However, the techniques embodied in this program are still limited by the altitude-Mach number combinations input into the program as points describing the approximate path, and yield nothing but a better approximation to the desired optimum path. The program is invaluable, though, as a generator of load factor as a function of time for input into the Bryson-Kelley Steepest Ascent Program as the nominal path.

This steepest-ascent method of optimization is an iterative scheme which begins with any non-optimal path and proceeds to derive a slight improvement each iteration from this nominal path. This slightly improved path at each iteration is used as the new nominal path, and the process is repeated until we are sufficiently close to the optimum for our purpose. In this process, each new path is found by taking the trajectory which yields the largest gain in performance for a given size of perturbation in the control variables.

The value of a good first guess at the nominal path is immediately evident. If this path is close to the optimum, the number of iterations necessary to arrive at this profile will be small indeed when compared to those necessary if the nominal path is far from the optimum. The ability to input good nominal paths results in tremendous savings of valuable computer time.

The analysis of single stage trajectories by the steepest ascent method has been thoroughly treated in the literature. One of the clearest treatments available is that of Bryson and Denham in Reference 2. For convenience, a brief description of the general problem, as formulated by them, is repeated here. Some of the detailed derivations which are omitted here are presented in Reference 2.

After presentation of the general problem, the specific applications made in formulating the program at the Air Proving Ground Center are given in detail.

GENERAL PROBLEM

Determine $\bar{x}(t)$ in the time interval $t_1 \leq t \leq t_2$, so as to maximize

$$(1) \quad \bar{J} = \bar{J}[\bar{x}(t_2), t_2]$$

subject to the constraints

$$(2) \quad \bar{V} = \bar{V}[\bar{x}(t_2), t_2] = 0$$

$$(3) \quad \frac{d\bar{x}}{dt} = \bar{f}[\bar{x}(t), \bar{u}(t), t]$$

$$(4) \quad \text{the given initial conditions } \bar{x}(t_1)$$

$$(5) \quad t_2 \text{ determined by } W = W[\bar{x}(t_2), t_2] = 0.$$

The bar over the symbols above indicates a matrix quantity, and a more detailed description of the above quantities follows:

$$(6) \quad \bar{u}(t) = \begin{bmatrix} u_1(t) \\ u_2(t) \\ \vdots \\ u_n(t) \end{bmatrix}, \text{ an } n \times 1 \text{ matrix of control variable programs, which we are free to choose,}$$

$$(7) \quad \bar{x}(t) = \begin{bmatrix} x_1(t) \\ x_2(t) \\ \vdots \\ x_n(t) \end{bmatrix}, \text{ an } n \times 1 \text{ matrix of state variable programs, resulting from the choice of } \bar{u}(t) \text{ and } \bar{x}(t_1),$$

$$(8) \quad \bar{\psi} = \begin{bmatrix} \psi_1 \\ \psi_2 \\ \vdots \\ \psi_p \end{bmatrix}, \text{ a } p \times 1 \text{ matrix of terminal constraint functions, each} \\ \text{a known function of } \bar{x}(t_2) \text{ and } t_2,$$

(9) ψ = the pay-off function, a known function of $\bar{x}(t_2)$ and t_2 ,

$$(10) \quad \bar{F} = \begin{bmatrix} f_1 \\ f_2 \\ \vdots \\ f_n \end{bmatrix}, \text{ an } n \times 1 \text{ matrix of known functions of } \bar{x}(t), \bar{u}(t), \text{ and } t, \\ \text{and}$$

(11) $\Omega = 0$ is the stopping condition that determines final time t_2 , and is a known function of $\bar{x}(t_2)$ and t_2 .

The method proceeds as follows:

1. Choose a reasonable nominal control variable program, $\bar{u}^*(t)$, and use it with the initial conditions (4) and the differential equations (3) to calculate, by numerical methods, the state variable programs $\bar{x}^*(t)$ until $\Omega = 0$. In general, this nominal path will not satisfy the terminal conditions $\bar{\psi} = 0$, or yield the maximum possible value of ψ .

2. Consider small perturbations $\delta\bar{u}(t)$ about the nominal control variable program, $\bar{u}^*(t)$, where

$$(12) \quad \delta\bar{u}(t) = \bar{u}(t) - \bar{u}^*(t).$$

As a result of these perturbations, the state variable programs undergo perturbations $\delta\bar{x}(t)$, where

$$(13) \quad \delta\bar{x}(t) = \bar{x}(t) - \bar{x}^*(t).$$

If the relations (12) and (13) are substituted into the differential equations, given by (3), the linear differential equations

$$(14) \quad \frac{d}{dt} (\delta\bar{x}) = \bar{F}(t)\delta\bar{x} + \bar{G}(t)\delta\bar{u}$$

are obtained, accurate to first order in the perturbations, where

$$(15) \quad \bar{F}(t) = \frac{\partial \bar{F}}{\partial \bar{x}} = \begin{bmatrix} \left(\frac{\partial f_1}{\partial x_1}\right)^* & \left(\frac{\partial f_1}{\partial x_2}\right)^* & \dots & \left(\frac{\partial f_1}{\partial x_n}\right)^* \\ \left(\frac{\partial f_2}{\partial x_1}\right)^* & \left(\frac{\partial f_2}{\partial x_2}\right)^* & \dots & \left(\frac{\partial f_2}{\partial x_n}\right)^* \\ \vdots & \vdots & \ddots & \vdots \\ \left(\frac{\partial f_m}{\partial x_1}\right)^* & \left(\frac{\partial f_m}{\partial x_2}\right)^* & \dots & \left(\frac{\partial f_m}{\partial x_n}\right)^* \end{bmatrix}$$

$$(16) \quad \bar{G}(t) = \frac{\partial \bar{F}}{\partial \bar{\sigma}} = \begin{bmatrix} \left(\frac{\partial f_1}{\partial \sigma_1}\right)^* & \left(\frac{\partial f_1}{\partial \sigma_2}\right)^* & \dots & \left(\frac{\partial f_1}{\partial \sigma_n}\right)^* \\ \left(\frac{\partial f_2}{\partial \sigma_1}\right)^* & \left(\frac{\partial f_2}{\partial \sigma_2}\right)^* & \dots & \left(\frac{\partial f_2}{\partial \sigma_n}\right)^* \\ \vdots & \vdots & \ddots & \vdots \\ \left(\frac{\partial f_m}{\partial \sigma_1}\right)^* & \left(\frac{\partial f_m}{\partial \sigma_2}\right)^* & \dots & \left(\frac{\partial f_m}{\partial \sigma_n}\right)^* \end{bmatrix}$$

The symbol ()^{*} indicates that the enclosed partial derivatives are evaluated along the nominal path.

Using the theory of adjoint differential equations, the following expressions may be written,

$$(17) \quad d\bar{x} = \int_{t_1}^{t_2} \bar{\lambda}'_x(t) \bar{G}(t) \delta \bar{\alpha}(t) dt + \bar{\lambda}'_x(t_1) \delta \bar{x}(t_1) + \dot{\bar{x}} dt_2$$

$$(18) \quad d\bar{y} = \int_{t_1}^{t_2} \bar{\lambda}'_y(t) \bar{G}(t) \delta \bar{\alpha}(t) dt + \bar{\lambda}'_y(t_1) \delta \bar{x}(t_1) + \dot{\bar{y}} dt_2$$

$$(19) \quad d\bar{z} = \int_{t_1}^{t_2} \bar{\lambda}'_z(t) \bar{G}(t) \delta \bar{\alpha}(t) dt + \bar{\lambda}'_z(t_1) \delta \bar{x}(t_1) + \dot{\bar{z}} dt_2,$$

where the symbol ' indicates the transpose of the matrix and elements of the three $\bar{\lambda}$ matrices, appearing above, are obtained through the numerical integration of the differential equations adjoint to equations (3):

$$(20) \quad \frac{d\bar{\lambda}}{dt} = -\bar{F}'(t)\bar{\lambda}(t)$$

with the boundary conditions

$$(21) \quad \bar{\lambda}_x'(t_2) = \left(\frac{\partial \phi}{\partial \bar{x}} \right)_{t=t_2}^*, \quad \bar{\lambda}_y'(t_2) = \left(\frac{\partial \bar{f}}{\partial \bar{x}} \right)_{t=t_2}^*, \quad \bar{\lambda}_\Omega'(t_2) = \left(\frac{\partial \Omega}{\partial \bar{x}} \right)_{t=t_2}^*,$$

where

$$(22) \quad \frac{\partial \phi}{\partial \bar{x}} = \left[\begin{array}{cccc} \frac{\partial \phi}{\partial x_1} & \frac{\partial \phi}{\partial x_2} & \dots & \frac{\partial \phi}{\partial x_n} \end{array} \right],$$

$$\frac{\partial \bar{f}}{\partial \bar{x}} = \left[\begin{array}{cccc} \frac{\partial \bar{f}_1}{\partial x_1} & \frac{\partial \bar{f}_1}{\partial x_2} & \dots & \frac{\partial \bar{f}_1}{\partial x_n} \\ \frac{\partial \bar{f}_2}{\partial x_1} & \frac{\partial \bar{f}_2}{\partial x_2} & \dots & \frac{\partial \bar{f}_2}{\partial x_n} \\ \vdots & \vdots & \vdots & \vdots \\ \frac{\partial \bar{f}_p}{\partial x_1} & \frac{\partial \bar{f}_p}{\partial x_2} & \dots & \frac{\partial \bar{f}_p}{\partial x_n} \end{array} \right]$$

$$\frac{\partial \Omega}{\partial \bar{x}} = \left[\begin{array}{cccc} \frac{\partial \Omega}{\partial x_1} & \frac{\partial \Omega}{\partial x_2} & \dots & \frac{\partial \Omega}{\partial x_n} \end{array} \right]$$

and

$$(23) \quad \dot{f} = \left(\frac{\partial \phi}{\partial t} + \frac{\partial \phi}{\partial \bar{x}} \bar{f} \right)_{t=t_2}^*, \quad \dot{f} = \left(\frac{\partial \bar{f}}{\partial t} + \frac{\partial \bar{f}}{\partial \bar{x}} \bar{f} \right)_{t=t_2}^*,$$

$$\dot{\Omega} = \left(\frac{\partial \Omega}{\partial t} + \frac{\partial \Omega}{\partial \bar{x}} \bar{f} \right)_{t=t_2}^*.$$

Note that the $\bar{\lambda}$'s are influence functions in that they tell how much a certain terminal condition is changed by a small change in some initial state variable. Note also that the adjoint equations (20) must be integrated backwards since the boundary conditions (21) are given at the terminal point.

For steepest ascent the $\delta\bar{\alpha}(t)$ program that maximizes the $d\bar{J}$ in expression (17) must be found, given values of $d\bar{y}$ and $d\Omega = 0$ in expressions (18) and (19), respectively. This maximization must also be subject to a given value of the integral

$$(24) \quad (dP)^2 = \int_{t_1}^{t_2} \delta\bar{\alpha}'(t) \bar{W}(t) \delta\bar{\alpha}(t) dt.$$

The value of $(dP)^2$ is chosen such that the perturbations will be small enough to insure that the neglect of second and higher order perturbations leading to equation (14) is reasonable. In addition, values of $d\bar{y}$ are selected to bring the next solution closer to the desired terminal constraints, $\bar{y} = 0$.

The $m \times n$ matrix $\bar{W}(t)$ is symmetric and contains weighting functions as elements. They may be chosen arbitrarily to improve convergence. In the usual case (the APGC program falls into this category), $\bar{W}(t)$ is taken equal to the identity matrix and $(dP)^2$ becomes the integral of the square of the control variable perturbations, $\delta\bar{\alpha}(t)$. Observation reveals that all control variables should have the same dimensions for equation (24) to have any meaning. To meet this requirement the control variables are normally required to be nondimensional.

A rather involved series of mathematical manipulations (presented in an orderly and clear fashion in Reference 2, but omitted here for the sake of brevity) leads to the following proper choice of $\delta\bar{\alpha}(t)$:

$$(25) \quad \delta\bar{\alpha}(t) = \pm \bar{W}^{-1} \bar{G}' \left(\bar{\lambda}_{\Omega} - \bar{\lambda}_{\Psi} \bar{I}^{-1} \bar{I} \right) \sqrt{\frac{(dP)^2 - d\bar{y}' \bar{I}^{-1} d\bar{y}}{1 - \bar{I}' \bar{I}^{-1} \bar{I}}} + \bar{W}^{-1} \bar{G}' \bar{\lambda}_{\Omega} \bar{I}^{-1} d\bar{y},$$

where

$$(26) \quad d\bar{y} = d\bar{y} - \bar{\lambda}'_{\Psi} (t_2) \delta\bar{x}(t_2),$$

$$(27) \quad \bar{\lambda}_{\Omega} = \bar{\lambda}_{\Psi} - \frac{\dot{\bar{y}}(t_2)}{\dot{\bar{x}}(t_2)} \bar{\lambda}_{\Omega},$$

$$(28) \quad \bar{\lambda}_{\Psi} = \bar{\lambda}_{\Psi} - \frac{\dot{\bar{y}}(t_2)}{\dot{\bar{x}}(t_2)} \bar{\lambda}_{\Omega},$$

$$(29) \quad \bar{I}_{\Psi\Psi} = \int_{t_1}^{t_2} \bar{\lambda}'_{\Omega} \bar{G} \bar{W}^{-1} \bar{G}' \bar{\lambda}_{\Omega} dt,$$

$$(30) \quad \bar{I}_{\psi\psi} = \int_{t_1}^t \bar{\lambda}'_{\psi\Omega} \bar{G} \bar{W}^{-1} \bar{G}' \bar{\lambda}_{\psi\Omega} dt,$$

$$(31) \quad I_{\psi\psi} = \int_{t_1}^t \lambda'_{\psi\Omega} \bar{G} \bar{W}^{-1} \bar{G}' \lambda_{\psi\Omega} dt,$$

and the $()^{-1}$ indicates the inverse matrix, and the + or - sign before the radical in (25) is chosen if ψ is to be increased or decreased, respectively.

If the selected $d\bar{\psi}$ is such that $d\bar{\beta}$ is too large, then the numerator in the radical in (25) might become negative and a limit to the size of $d\bar{\beta}$ for a given dP must be imposed. Since dP is chosen to insure valid linearization, the selected $d\bar{\beta}$ must also be limited.

The predicted change in ψ for the change in $\bar{\alpha}(t)$ given by (25) is

$$(32) \quad d\psi = \pm \sqrt{[(dP)^2 - d\bar{\beta}' \bar{I}_{\psi\psi}^{-1} d\bar{\beta}] [I_{\psi\psi} - \bar{I}'_{\psi\psi} \bar{I}^{-1} \bar{I}_{\psi\psi}]} + \bar{I}'_{\psi\psi} \bar{I}^{-1} d\bar{\beta} + \bar{\lambda}'_{\psi\Omega}(t_1) \delta\bar{x}(t_1).$$

If $d\bar{\psi} = 0$ (the terminal constraints having been satisfied) and $\delta\bar{x}(t_1) = 0$, then $d\bar{\beta} = 0$ and equation (32) becomes

$$(33) \quad \frac{d\psi}{dP} = \pm \sqrt{I_{\psi\psi} - \bar{I}'_{\psi\psi} \bar{I}^{-1} \bar{I}_{\psi\psi}},$$

which is a gradient in function space, since dP is the length of the step in the control variable program. As the optimum program is approached and the terminal constraints are met, ($d\bar{\psi} = 0$), this gradient must tend to zero, and expression (32) becomes

$$(34) \quad d\psi = \bar{I}'_{\psi\psi} \bar{I}^{-1} d\bar{\beta} + [\bar{\lambda}'_{\psi\Omega}(t_1) - \bar{I}'_{\psi\psi} \bar{I}^{-1} \bar{\lambda}'_{\psi\Omega}(t_1)] \delta\bar{x}(t_1)$$

3. A new control variable program is now obtained as

$$(35) \quad \bar{\alpha}(t) = \bar{\alpha}^*(t) + \delta\bar{\alpha}(t).$$

This new $\bar{\alpha}(t)$ is now used in the original nonlinear differential equation given by (3), and the process is repeated until the terminal constraints (2) are met and the gradient (33) becomes nearly zero.

THE EGLIN PROGRAM

During the spring of 1964, preparations were begun for the physical test to validate the Energy-Maneuverability theory, as requested by the Tactical Air Command. The test was designed to show that the "dipsy-doodle" maneuvers associated with minimum time-to-climb and minimum fuel paths did, in fact, represent the optimum flight profiles for transfer from one energy level to another. The above test was conducted under APCC Project 0570T1.

To adequately support this test, a program which could compute these optimum paths was necessary. Arrangements had been made to obtain the Bryson-Kelley Steepest Ascent Computer Program from the Flight Dynamics Laboratory at Wright-Patterson AFB. The program was being formulated and developed under Contract No. AF 33(657)-8829 by McDonnell Aircraft Corporation. When advised that this program would not be ready in time for the test, the decision was made to develop a program in-house at Eglin. Due to time limitations, a somewhat simple Bryson-Kelley Steepest Ascent Program was formulated in two dimensions and with one control variable.

The program was completed in August 1964 and used extensively during the conduct of the test. Before giving the details of the Eglin formulation, an explanation of some key features of the program which are not provided in the general formulation will be presented.

As mentioned before, the program has but one control variable, n , the normal acceleration in number of g 's. Originally, the program was formulated with velocity and pitch angle serving as terminal constraints v_1 and ψ_1 with altitude as the stopping condition Ω . However, using two terminal constraints led to trouble with the matrix $\ddot{I}_{\psi\psi}$. This matrix was found to be nearly singular, and the existence of its inverse was, therefore, quite questionable.

Analysis revealed that the constraint on pitch angle was not vital and that two programs should be developed: one with velocity serving as the terminal constraint with altitude in the role of stopping condition, and the other with the roles of velocity and altitude reversed.

In reducing the application of the Steepest Ascent Method to a routine computation, an automatic scheme or control system for determining the step size, $(dP)^2$, must be devised. In the Eglin program, this control system is as follows:

1. Begin with a desired improvement in the quantity to be optimized (time for minimum time paths and total weight for minimum fuel paths). This desired improvement, $d\phi$, should be reflected in the next iteration if the terminal constraint has been met. Equation (32) is solved for $(dP)^2 = d\beta' \ddot{I}_{\psi\psi}^{-1} d\beta$ as a function of the given $d\phi$.

2. If the terminal constraint has not been met, check to see if $(dP)^2 - d\bar{P}'\bar{I}_\psi^{-1}d\bar{P} < 0$. If so, scale down $d\bar{y}$ such that the quantity is zero. If not, use the $(dP)^2 - d\bar{P}'\bar{I}_\psi^{-1}d\bar{P}$, obtained from expression (32), in the expression for $\delta\bar{x}(t)$ given in (25).

3. The requested $d\bar{y}$ is then modified as each iteration comes closer to the optimum. This modification is controlled by the magnitude of the gradient given by (33). As this magnitude grows smaller and becomes less than predetermined values, the size of $d\bar{y}$ is successively halved. The given values of the gradient, at which the $d\bar{y}$'s are halved, are not readily obvious and appropriate values must be learned through some experience with the program.

4. Even with this semiautomatic control device, considerable time must be spent in determining values of the gradient with the possibility that considerable computer time may still be consumed before a true optimum path is reached. Several other control systems are presently under investigation at Eglin AFB. It is hoped that a better automatic scheme will be found which will decrease both computer running time and the manpower required to eventually arrive at the optimum paths.

The formulation of the Bryson-Kelley technique, presently in use at Eglin AFB, is presented here such that one may readily follow it, having been made acquainted with the general problem previously.

1. Control Variable Matrix $\bar{x}(t)$. (m x 1) Matrix

$$\bar{x}(t) = n(t),$$

where $m = 1$ and $n =$ normal acceleration in number of g's (dimensionless).

2. State Variable Matrix $\bar{z}(t)$. (n x 1) Matrix

$$\bar{z}(t) = \begin{bmatrix} x_1 \\ x_2 \\ x_3 \\ x_4 \end{bmatrix} = \begin{bmatrix} h(t) \\ V(t) \\ \gamma(t) \\ w(t) \end{bmatrix}, \text{ where } n = 4,$$

$h =$ altitude above MSL in feet,

$V =$ true airspeed in feet per second,

$\gamma =$ pitch angle (angle between velocity vector and reference horizontal plane) in radians,

$w =$ aircraft gross weight in pounds.

3. Terminal Constraint Matrix $\bar{F} = 0$. (p x 1) Matrix
- a. $\bar{F} = \dot{h} = h - h_2$ for Program 556, where h is terminal (p = 1) constraint and V is stopping condition.
- b. $\bar{F} = \dot{V} = V - V_2$ for Program 623, where V is terminal (p = 1) constraint and h is stopping condition.

h_2 = desired terminal altitude in feet,

V_2 = desired terminal velocity in feet per second.

4. Pay-Off Function ϕ

a. $\phi = -t$ for minimum time paths.

b. $\phi = w$ for minimum fuel paths.

5. Time Derivative of State Variable Matrix, \bar{F} . (n x 1) Matrix

$$\bar{F} [\bar{x}, n, t] = \frac{d\bar{x}}{dt}$$

$$\bar{F} [\bar{x}, n, t] = \begin{bmatrix} \dot{x}_1 \\ f_2 \\ f_3 \\ f_4 \end{bmatrix} = \begin{bmatrix} \dot{x}_1 \\ \dot{x}_2 \\ \dot{x}_3 \\ \dot{x}_4 \end{bmatrix} = \begin{bmatrix} \dot{h} \\ \dot{V} \\ \dot{\gamma} \\ \dot{\omega} \end{bmatrix}. \quad (n = 4).$$

a. $f_1 = \dot{h} = V \sin \gamma,$

$$f_2 = \dot{V} = g \left[\frac{T_a - D}{w} - \sin \gamma \right],$$

$$f_3 = \dot{\gamma} = \frac{g}{V} [n - \cos \gamma],$$

$$f_4 = \dot{\omega} = -\dot{\omega},$$

where

g = acceleration of gravity = 32.174 ft/sec²,

T_a = thrust available in pounds,

D = drag in pounds,

$\dot{\omega}$ = fuel flow in pounds per second.

6. Stopping Condition $\Omega = 0$.

a. $\Omega = V - V_2$, for Program 556.

b. $\Omega = h - h_2$, for Program 623.

7. $\bar{F}(t) = \frac{\partial \bar{f}(t)}{\partial \bar{x}(t)}$ (n x n) Matrix

$\bar{f}(t) = [f_{ij}(t)]$, $i, j = 1, 2, \dots, n$.

$f_{ij} = \frac{\partial f_i}{\partial x_j} = \frac{\partial \dot{x}_i}{\partial x_j}$

a. $f_{11} = \frac{\partial \dot{h}}{\partial h} = \frac{\partial (V \sin \gamma)}{\partial h} = 0$, (n = 4)

b. $f_{12} = \frac{\partial \dot{h}}{\partial V} = \sin \gamma$,

c. $f_{13} = \frac{\partial \dot{h}}{\partial \gamma} = V \cos \gamma$,

d. $f_{14} = \frac{\partial \dot{h}}{\partial w} = 0$,

e. $f_{21} = \frac{\partial \dot{V}}{\partial h} = \frac{\partial \left\{ \frac{g(T_2 - D)}{w} - \sin \gamma \right\}}{\partial h} = \frac{g}{w} \frac{\partial (T_2 - D)}{\partial h}$,

f. $f_{22} = \frac{\partial \dot{V}}{\partial V} = \frac{g}{w} \frac{\partial (T_2 - D)}{\partial V}$,

g. $f_{23} = \frac{\partial \dot{V}}{\partial \gamma} = -g \cos \gamma$,

h. $f_{24} = \frac{\partial \dot{V}}{\partial w} = -\frac{g}{w} \left\{ \frac{T_2 - D}{w} + \frac{\partial D}{\partial w} \right\}$,

i. $f_{31} = \frac{\partial \dot{\gamma}}{\partial h} = \frac{\partial \left\{ \frac{g}{V} (n - \cos \gamma) \right\}}{\partial h} = 0$,

j. $f_{32} = \frac{\partial \dot{\gamma}}{\partial V} = -\frac{g}{V^2} (n - \cos \gamma)$,

$$k. f_{33} = \frac{\partial \dot{\gamma}}{\partial \gamma} = \frac{g}{v} \sin \gamma,$$

$$l. f_{34} = \frac{\partial \dot{\gamma}}{\partial w} = 0,$$

$$m. f_{41} = \frac{\partial \dot{w}}{\partial h} = -\frac{\partial \dot{h}}{\partial h},$$

$$n. f_{42} = \frac{\partial \dot{w}}{\partial v} = -\frac{\partial \dot{v}}{\partial v},$$

$$o. f_{43} = \frac{\partial \dot{w}}{\partial \gamma} = 0,$$

$$p. f_{44} = \frac{\partial \dot{w}}{\partial w} = 0.$$

$$8. \bar{G}(t) = \frac{\partial \bar{f}(t)}{\partial \bar{Q}(t)} \quad (n \times m) \text{ Matrix}$$

$$\bar{G}(t) = \frac{\partial \bar{f}(t)}{\partial n} = \left[\frac{\partial f_i}{\partial n} \right], \quad i = 1, \dots, 4. \quad \begin{pmatrix} n = 4 \\ m = 1 \end{pmatrix}$$

Let

$$\bar{G}(t) = [g_i] \quad i = 1, \dots, 4,$$

$$a. g_1 = \frac{\partial \dot{h}}{\partial n} = \frac{\partial [v \sin \gamma]}{\partial n} = 0,$$

$$b. g_2 = \frac{\partial \dot{v}}{\partial n} = \frac{\partial \left\{ g \frac{r_a - D}{w} - \sin \gamma \right\}}{\partial n} = -\frac{g}{w} \frac{\partial D}{\partial n},$$

$$c. g_3 = \frac{\partial \dot{\gamma}}{\partial n} = \frac{\partial \left\{ \frac{g}{v} (n - \cos \gamma) \right\}}{\partial n} = \frac{g}{v},$$

$$d. g_4 = \frac{\partial \dot{w}}{\partial n} = -\frac{\partial \dot{h}}{\partial n} = 0.$$

9. Lagrange Multipliers.

$$a. \quad \bar{\lambda}_q = \begin{bmatrix} \lambda_{q1} \\ \lambda_{q2} \\ \lambda_{q3} \\ \lambda_{q4} \end{bmatrix},$$

$$b. \quad \bar{\lambda}_p = \begin{bmatrix} \lambda_{p1} \\ \lambda_{p2} \\ \lambda_{p3} \\ \lambda_{p4} \end{bmatrix},$$

$$c. \quad \bar{\lambda}_\Omega = \begin{bmatrix} \lambda_{\Omega 1} \\ \lambda_{\Omega 2} \\ \lambda_{\Omega 3} \\ \lambda_{\Omega 4} \end{bmatrix}.$$

10. Adjoint Differential Equations for Lagrange Multipliers,

$$a. \quad \frac{d\bar{\lambda}_q}{dt} = -\bar{F}'\bar{\lambda}_q,$$

$$b. \quad \frac{d\bar{\lambda}_p}{dt} = -\bar{F}'\bar{\lambda}_p,$$

$$c. \quad \frac{d\bar{\lambda}_\Omega}{dt} = -\bar{F}'\bar{\lambda}_\Omega.$$

Now

$$\bar{F}' = \begin{bmatrix} 0 & f_{21} & 0 & f_{41} \\ f_{12} & f_{22} & f_{32} & f_{42} \\ f_{13} & f_{23} & f_{33} & 0 \\ 0 & f_{24} & 0 & 0 \end{bmatrix}$$

where the f_{ij} are given in (7).

Performing the matrix multiplications indicated in 7a, 7b, and 7c, we have the following set of differential equations for the individual elements of the Lagrange Multiplier matrices:

$$d. \quad \dot{\lambda}_{qj} = -\sum_{i=1}^4 \lambda_{qi} f_{ij}, \quad j = 1, 2, 3, 4.$$

$$(1) \dot{\lambda}_{\theta_1} = -(\lambda_{\theta_2} f_{21} + \lambda_{\theta_4} f_{41}),$$

$$(2) \dot{\lambda}_{\theta_2} = -(\lambda_{\theta_1} f_{12} + \lambda_{\theta_3} f_{32} + \lambda_{\theta_4} f_{42}),$$

$$(3) \dot{\lambda}_{\theta_3} = -(\lambda_{\theta_2} f_{23} + \lambda_{\theta_4} f_{43}),$$

$$(4) \dot{\lambda}_{\theta_4} = -\lambda_{\theta_2} f_{24}.$$

$$e. \quad \lambda_{\theta_j} = -\sum_{i=1}^4 \lambda_{\theta_i} f_{ij}, \quad j = 1, 2, 3, 4.$$

$$(1) \dot{\lambda}_{\theta_1} = -(\lambda_{\theta_2} f_{21} + \lambda_{\theta_4} f_{41}).$$

$$(2) \dot{\lambda}_{\theta_2} = -(\lambda_{\theta_1} f_{12} + \lambda_{\theta_3} f_{32} + \lambda_{\theta_4} f_{42}).$$

$$(3) \dot{\lambda}_{\theta_3} = -(\lambda_{\theta_2} f_{23} + \lambda_{\theta_4} f_{43}).$$

$$(4) \dot{\lambda}_{\theta_4} = -\lambda_{\theta_2} f_{24}.$$

$$f. \quad \dot{\lambda}_{\theta_j} = -\sum_{i=1}^4 \lambda_{\theta_i} f_{ij}, \quad j = 1, 2, 3, 4.$$

$$(1) \dot{\lambda}_{\theta_1} = -(\lambda_{\theta_2} f_{21} + \lambda_{\theta_4} f_{41}).$$

$$(2) \dot{\lambda}_{\theta_2} = -(\lambda_{\theta_1} f_{12} + \lambda_{\theta_3} f_{32} + \lambda_{\theta_4} f_{42}).$$

$$(3) \dot{\lambda}_{\theta_3} = -(\lambda_{\theta_2} f_{23} + \lambda_{\theta_4} f_{43}).$$

$$(4) \dot{\lambda}_{\theta_4} = -\lambda_{\theta_2} f_{24}.$$

11. Boundary Conditions for Lagrange Multipliers.

$$a. \quad \bar{\lambda}_i(t_2) = \left[\frac{\partial \bar{f}}{\partial x_i} \right]_{t=t_2}, \text{ or } \dot{\lambda}_i(t_2) = \left(\frac{\partial \bar{f}}{\partial x_i} \right)_{t=t_2}, \quad i = 1, 2, 3, 4.$$

(1) For maximizing $\bar{f} = -t$ (minimum time paths).

$$\lambda_{\phi}(t_2) = \begin{bmatrix} -\frac{\partial t}{\partial h} \\ -\frac{\partial t}{\partial V} \\ -\frac{\partial t}{\partial \gamma} \\ -\frac{\partial t}{\partial w} \end{bmatrix} = \begin{bmatrix} 0 \\ 0 \\ 0 \\ 0 \end{bmatrix},$$

or

$$\lambda_{\phi_1}(t_2) = \lambda_{\phi_2}(t_2) = \lambda_{\phi_3}(t_2) = \lambda_{\phi_4}(t_2) = 0.$$

(2) For maximizing $\phi = w$ (minimum fuel paths),

$$\lambda_{\phi}(t_2) = \begin{bmatrix} \frac{\partial w}{\partial h} \\ \frac{\partial w}{\partial V} \\ \frac{\partial w}{\partial \gamma} \\ \frac{\partial w}{\partial w} \end{bmatrix}_{t=t_2} = \begin{bmatrix} 0 \\ 0 \\ 0 \\ 1 \end{bmatrix}.$$

or

$$\lambda_{\phi_1}(t_2) = \lambda_{\phi_2}(t_2) = \lambda_{\phi_3}(t_2) = 0, \text{ and } \lambda_{\phi_4}(t_2) = 1.$$

$$b. \quad \bar{\lambda}_{\phi}(t_2) = \left[\frac{\partial \phi}{\partial x_i} \right]_{t=t_2}, \text{ or } \lambda_{\phi_i}(t_2) = \left[\frac{\partial \phi}{\partial x_i} \right]_{t=t_2}, \quad i = 1, 2, 3, 4.$$

(1) For terminal constraint on h (Program 556),

$$\bar{\lambda}_\psi(t_2) = \begin{bmatrix} \frac{\partial h}{\partial h} \\ \frac{\partial h}{\partial V} \\ \frac{\partial h}{\partial Y} \\ \frac{\partial h}{\partial w} \end{bmatrix}_{t=t_2} = \begin{bmatrix} 1 \\ 0 \\ 0 \\ 0 \end{bmatrix},$$

or

$$\lambda_{\psi_1}(t_2) = 1, \text{ and } \lambda_{\psi_2}(t_2) = \lambda_{\psi_3}(t_2) = \lambda_{\psi_4}(t_2) = 0.$$

(2) For terminal constraint on V (Program 623),

$$\bar{\lambda}_\psi(t_2) = \begin{bmatrix} \frac{\partial V}{\partial h} \\ \frac{\partial V}{\partial V} \\ \frac{\partial V}{\partial Y} \\ \frac{\partial V}{\partial w} \end{bmatrix}_{t=t_2} = \begin{bmatrix} 0 \\ 1 \\ 0 \\ 0 \end{bmatrix},$$

or

$$\lambda_{\psi_2}(t_2) = 1, \text{ and } \lambda_{\psi_1}(t_2) = \lambda_{\psi_3}(t_2) = \lambda_{\psi_4}(t_2) = 0.$$

c. $\bar{\lambda}_{\gamma_i}(t_2) = \left[\frac{\partial \eta}{\partial x_i} \right]_{t=t_2}$, or $\lambda_{\gamma_i}(t_2) = \left[\frac{\partial \eta}{\partial x_i} \right]_{t=t_2}$, $i = 1, 2, 3, 4$.

(1) For Stopping Condition on V (Program 556),

$$\bar{\lambda}_{\Omega}(t_2) = \begin{bmatrix} \frac{\partial V}{\partial h} \\ \frac{\partial V}{\partial V} \\ \frac{\partial V}{\partial Y} \\ \frac{\partial V}{\partial w} \end{bmatrix}_{t=t_2} = \begin{bmatrix} 0 \\ 1 \\ 0 \\ 0 \end{bmatrix},$$

or

$$\lambda_{\Omega_2}(t_2) = 1, \text{ and } \lambda_{\Omega_3}(t_2) = \lambda_{\Omega_4}(t_2) = \lambda_{\Omega_5}(t_2) = 0.$$

(2) For Stopping Condition on h (Program 623),

$$\bar{\lambda}_{\Omega}(t_2) = \begin{bmatrix} \frac{\partial h}{\partial h} \\ \frac{\partial h}{\partial V} \\ \frac{\partial h}{\partial Y} \\ \frac{\partial h}{\partial w} \end{bmatrix}_{t=t_2} = \begin{bmatrix} 1 \\ 0 \\ 0 \\ 0 \end{bmatrix},$$

or

$$\lambda_{\Omega_1}(t_2) = 1, \text{ and } \lambda_{\Omega_2}(t_2) = \lambda_{\Omega_3}(t_2) = \lambda_{\Omega_4}(t_2) = 0.$$

12. The Matrices $\bar{\lambda}_{\Omega_1}$ and $\bar{\lambda}_{\Omega_2}$.

$$a. \quad \bar{\lambda}_{\Omega_1} = \bar{\lambda}_2 - \frac{\dot{h}(t_2)}{\dot{\Omega}(t_2)} \bar{\lambda}_{\Omega_2}$$

or

$$\lambda_{\psi_i} = \lambda_{\psi_1} - \frac{\dot{\psi}(t_2)}{\dot{\chi}(t_2)} \lambda_{\Omega_i}, \quad i = 1, 2, 3, 4.$$

(1) For maximizing $\psi = -t$ (minimum time paths),

$$\dot{\psi}(t_2) = -1.$$

(2) For maximizing $\psi = w$ (minimum fuel paths),

$$\dot{\psi}(t_2) = -\dot{w}(t_2)$$

(3) For Stopping Condition on V (Program 556),

$$\dot{\chi}(t_2) = \dot{V}(t_2) = g \left\{ \frac{T_A - D}{w} - \sin \gamma \right\} \quad t = t_2.$$

(4) For Stopping Condition on h (Program 623),

$$\dot{\chi}(t_2) = \dot{h}(t_2) = \{V \sin \gamma\} \quad t = t_2.$$

$$b. \quad \bar{\lambda}_{\psi\Omega} = \bar{\lambda}_{\psi} - \frac{\dot{\psi}(t_2)}{\dot{\chi}(t_2)} \bar{\lambda}_{\Omega}$$

or

$$\lambda_{\psi\Omega_i} = \lambda_{\psi_i} - \frac{\dot{\psi}(t_2)}{\dot{\chi}(t_2)} \lambda_{\Omega_i}, \quad i = 1, 2, 3, 4.$$

(1) For terminal constraint on h (Program 556),

$$\dot{\psi}(t_2) = \dot{h}(t_2) = \{V \sin \gamma\} \quad t = t_2.$$

(2) For terminal constraint on V (Program 623),

$$\dot{\psi}(t_2) = \dot{V}(t_2) = g \left\{ \frac{T_A - D}{w} - \sin \gamma \right\} \quad t = t_2.$$

13. The Matrix Product $[\bar{\lambda}_{\psi\Omega}]' \bar{G}$.

$$[\bar{\lambda}_{\psi\Omega}]' \bar{G} = \sum_{i=1}^4 \lambda_{\psi\Omega_i} \bar{G}_i = \bar{G}' \bar{\lambda}_{\psi\Omega} = \lambda_{\psi\Omega_1} \bar{G}_1 + \lambda_{\psi\Omega_2} \bar{G}_2 + \lambda_{\psi\Omega_3} \bar{G}_3 + \lambda_{\psi\Omega_4} \bar{G}_4.$$

14. The Matrix Product $[\bar{\lambda}_{\psi\Omega}]' \bar{G}$.

$$[\bar{\lambda}_{\psi\Omega}]' \bar{G} = \sum_{i=1}^4 \lambda_{\psi\Omega_i} \bar{G}_i = \bar{G}' \bar{\lambda}_{\psi\Omega} = \lambda_{\psi\Omega_2} \bar{G}_2 + \lambda_{\psi\Omega_3} \bar{G}_3.$$

15. The Integrals $\bar{I}_{\psi\psi}$, $\bar{I}_{\psi\bar{\psi}}$, and $\bar{I}_{\bar{\psi}\bar{\psi}}$.

a.
$$\bar{I}_{\psi\psi} = \int_{t_1}^{t_2} [\bar{\lambda}_{\psi\Omega}]' \bar{G} [\bar{W}]^{-1} [\bar{G}]' \bar{\lambda}_{\psi\Omega} dt = \int_{t_1}^{t_2} [\lambda_{\psi\Omega_2} \bar{G}_2 + \lambda_{\psi\Omega_3} \bar{G}_3]' \bar{W} dt,$$

as $\bar{W} = 1$.

b.
$$\bar{I}_{\psi\bar{\psi}} = \int_{t_1}^{t_2} [\bar{\lambda}_{\psi\Omega}]' \bar{G} [\bar{W}]^{-1} [\bar{G}]' \bar{\lambda}_{\bar{\psi}\Omega} dt.$$

$$= \int_{t_1}^{t_2} [\lambda_{\psi\Omega_2} \bar{G}_2 + \lambda_{\psi\Omega_3} \bar{G}_3]' [\lambda_{\bar{\psi}\Omega_2} \bar{G}_2 + \lambda_{\bar{\psi}\Omega_3} \bar{G}_3] dt.$$

c.
$$\bar{I}_{\bar{\psi}\bar{\psi}} = \int_{t_1}^{t_2} [\bar{\lambda}_{\bar{\psi}\Omega}]' \bar{G} [\bar{W}]^{-1} [\bar{G}]' \bar{\lambda}_{\bar{\psi}\Omega} dt$$

$$= \int_{t_1}^{t_2} [\lambda_{\bar{\psi}\Omega_2} \bar{G}_2 + \lambda_{\bar{\psi}\Omega_3} \bar{G}_3]' \bar{W} dt.$$

16. The Matrix Product $d\bar{\beta}' \bar{I}_{\psi\psi}^{-1} d\bar{\beta}$.

$$d\bar{\beta} = d\bar{\psi} - \bar{\lambda}_{\psi\Omega}(t_1) \delta\bar{x}(t_1)$$

$$= d\bar{\psi} \text{ as } \delta\bar{x}(t_1) = 0.$$

a. $d\bar{\psi} = \Delta h$ for Program 556,

b. $d\bar{\psi} = \Delta V$ for Program 623,

where Δh and ΔV are the terminal condition changes necessary to bring the next solution closer to the desired terminal constraints.

c. $\Delta h = h_2 - h(t_2),$

d. $\Delta V = V_2 - V(t_2),$

where $h(t_2)$ and $V(t_2)$ are the altitude and true airspeed at the final time point, $t = t_2$, of the previous solution.

Combining the results from above,

$$d\beta' \bar{I}_{\psi\psi}^{-1} d\beta = \frac{(d\psi)^2}{I_{\psi\psi}}$$

17. The Matrix Product $\bar{I}'_{\psi\psi} \bar{I}_{\psi\psi}^{-1} \bar{I}_{\psi\psi}$.

Since the matrices $\bar{I}_{\psi\psi}$ and $\bar{I}'_{\psi\psi}$ are both one-by-one scalars,

$$\bar{I}'_{\psi\psi} \bar{I}_{\psi\psi}^{-1} \bar{I}_{\psi\psi} = \frac{(I_{\psi\psi})^2}{I_{\psi\psi}}$$

18. The Matrix Product $\bar{I}'_{\psi\psi} \bar{I}_{\psi\psi}^{-1} d\beta$.

$$\bar{I}'_{\psi\psi} \bar{I}_{\psi\psi}^{-1} d\beta = \frac{I_{\psi\psi} d\psi}{I_{\psi\psi}}$$

19. The Expression $(dP)^2 = d\beta' \bar{I}_{\psi\psi}^{-1} d\beta$.

From expression (32) is obtained the relationship

$$a. \quad (dP)^2 = d\beta' \bar{I}_{\psi\psi}^{-1} d\beta = \frac{[d\psi - \bar{I}'_{\psi\psi} \bar{I}_{\psi\psi}^{-1} d\beta]^2}{I_{\psi\psi} - \bar{I}'_{\psi\psi} \bar{I}_{\psi\psi}^{-1} \bar{I}_{\psi\psi}}$$

which can be reduced to the following expressions, using the results of previous paragraphs:

$$b. \quad (dP)^2 = d\beta' \bar{I}_{\psi\psi}^{-1} d\beta = \frac{\left[d\psi - \frac{I_{\psi\psi} d\psi}{I_{\psi\psi}} \right]^2}{I_{\psi\psi} - \frac{(I_{\psi\psi})^2}{I_{\psi\psi}}}$$

If the terminal constraint has been satisfied, that is,

$$c. \quad |\Delta h| \leq \xi_1 \quad \text{for Program 556, or}$$

$$d. \quad |\Delta V| \leq \xi_2 \quad \text{for Program 623,}$$

where ξ_1 is some predetermined tolerance within which the terminal constraint on altitude must fall, and ξ_2 , the tolerance for a terminal constraint on velocity, then the expression (19.a.) is used in the expression for $\delta\mathcal{E}(t)$.

If the value of $|\Delta h|$ or $|\Delta V|$ is outside the predetermined tolerance, then set $(dP)^2 - d\bar{P}' \bar{I}_{\psi\psi}^{-1} d\bar{P} = 0$, and use in the expression for $\delta\bar{z}(t)$.

20. The Matrix Product $\bar{W}^{-1} \bar{G}' (\bar{\lambda}_{\psi\Omega} - \bar{\lambda}_{\psi\Omega} \bar{I}_{\psi\psi}^{-1} \bar{I}_{\psi\psi})$.

$$\bar{W}^{-1} \bar{G}' (\bar{\lambda}_{\psi\Omega} - \bar{\lambda}_{\psi\Omega} \bar{I}_{\psi\psi}^{-1} \bar{I}_{\psi\psi}) = \xi_2 \left(\lambda_{\psi\Omega_2} - \frac{\lambda_{\psi\Omega_2} I_{\psi\psi}}{I_{\psi\psi}} \right) + \xi_3 \left(\lambda_{\psi\Omega_3} - \frac{\lambda_{\psi\Omega_3} I_{\psi\psi}}{I_{\psi\psi}} \right).$$

21. The Matrix Product $\bar{W}^{-1} \bar{G}' \bar{\lambda}_{\psi\Omega} \bar{I}_{\psi\psi}^{-1} d\bar{P}$.

$$\bar{W}^{-1} \bar{G}' \bar{\lambda}_{\psi\Omega} \bar{I}_{\psi\psi}^{-1} d\bar{P} = \frac{(\lambda_{\psi\Omega_2} \xi_2 + \lambda_{\psi\Omega_3} \xi_3)}{I_{\psi\psi}} d\psi.$$

22. The Expression for $\delta\bar{z}(t)$.

Combining the results of the preceding pages, the following expression for $\delta\bar{z}(t)$ is obtained:

$$\begin{aligned} \text{a. } \delta\bar{z}(t) = & \pm \left[\xi_2 \left(\lambda_{\psi\Omega_2} - \frac{\lambda_{\psi\Omega_2} I_{\psi\psi}}{I_{\psi\psi}} \right) \right] \\ & + \left[\xi_3 \left(\lambda_{\psi\Omega_3} - \frac{\lambda_{\psi\Omega_3} I_{\psi\psi}}{I_{\psi\psi}} \right) \right] \left[\frac{I_{\psi\psi} d\psi - I_{\psi\psi} d\psi}{I_{\psi\psi} I_{\psi\psi} - (I_{\psi\psi})^2} \right] \\ & + \frac{(\lambda_{\psi\Omega_2} \xi_2 + \lambda_{\psi\Omega_3} \xi_3)}{I_{\psi\psi}} d\psi. \end{aligned}$$

If the value of $|\Delta h|$ or $|\Delta V|$ is outside the tolerance, ξ_1 or ξ_3 , respectively, then

$$\text{b. } \delta\bar{z}(t) = \frac{(\lambda_{\psi\Omega_2} \xi_2 + \lambda_{\psi\Omega_3} \xi_3)}{I_{\psi\psi}} d\psi.$$

PART III. DYNAMIC PROFILE GENERATOR

The Dynamic Profile Generator uses the aerodynamic and performance data for a given aircraft to connect points in the altitude-Mach number plane with an approximate dynamic profile consistent with the capabilities and limitations of the aircraft. The program provides a time history of the normal acceleration, pitch angle, drag, fuel consumed, and horizontal range traversed throughout the flight path.

The program is designed to compute normal acceleration in number of g's as a function of time, associated with the dynamic profile necessary to fly through the altitude-Mach number points defining a Rutowski path for a given aircraft. This g schedule then serves as a good first guess for the nominal path in the Bryson-Kelley Steepest Ascent Program, leading to either a minimum time or minimum fuel path for transfer between different energy levels.

An initial aircraft gross weight, w_1 , normal acceleration, n_1 , and pitch angle, γ_1 , are assumed at the first altitude-Mach number point (h_1, M_1) of the path. The usual assumption is that the transfer between energy levels is initiated from level flight, i.e., $n_1 = 1.0$ g and $\gamma_1 = 0$. Figure II-2 depicts a typical path composed of N (h, M) points.

To obtain the values for the quantities at the i th point (h_i, M_i) , we employ an iterative predictor-corrector process involving two major steps: (1) predicting the value of some of the quantities across the interval from (h_{i-1}, M_{i-1}) to (h_i, M_i) based on known values from the former point and (2) correcting these values during each of a number of iterations until a desired level of convergence is attained.

The time interval and fuel consumed are estimated for the interval between the points, as discussed previously in this appendix, and either of two methods employed to determine the normal acceleration required by the aircraft to fly between the points.

The first method involves solving simultaneously the equations of motion along and perpendicular to the path to provide an expression for the coefficient of lift, C_L :

$$\bar{C}_L = \Delta \bar{C}_L + \sqrt{\frac{\bar{T}_e - \bar{w} (\sin \bar{\gamma} + \dot{V}/g)}{\bar{q} S K} - \frac{\bar{C}_{D_e}}{\bar{K}}}$$

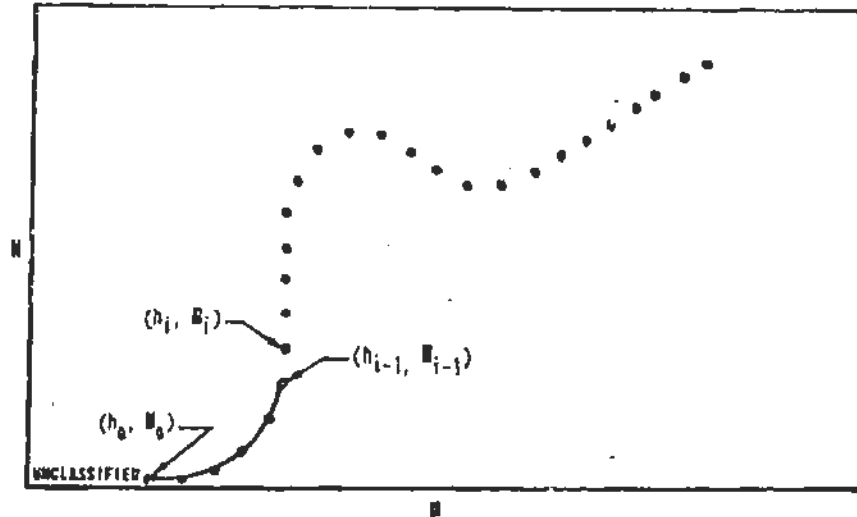


Figure 11-2. Typical Rutowski Path Used by the Dynamic Profile Generator.

where C_{D_0} is the zero-lift drag coefficient,

- K is the induced drag parameter,
- ΔC_L is the value of C_L for which C_D is minimum
- T_a is the thrust available in pounds,
- w is the aircraft gross weight in pounds,
- γ is the aircraft pitch angle,
- \dot{v} is the acceleration along the flight path in ft/sec^2 ,
- g is the acceleration due to gravity,
- q is the dynamic pressure in lb/ft^2 ,
- S is the aircraft reference wing area in ft^2 .

The bar notation (\bar{C}_L or \bar{T}_a) indicates the value of this quantity at the midpoint of the interval.

The pitch angle ($\bar{\gamma}$) at this midpoint is approximated by the following expression:

$$\sin \bar{\gamma} = \frac{h_i - h_{i-1}}{V \Delta t}$$

~~CONFIDENTIAL~~

where Δt is the time increment required to fly between (h_{i-1}, M_{i-1}) and (h_i, M_i) . This value for $\sin \bar{\gamma}$ along with the other required information are used to determine \bar{C}_L which provides the value of n , the normal acceleration in number of g's across the interval.

An alternate method employs an estimate of $\sin \gamma_i$ by the expression:

$$\sin \gamma_i = \frac{2\Delta h}{V\Delta t}$$

to obtain the angular rate $\dot{\gamma}$:

$$\dot{\gamma} = \frac{\gamma_i - \gamma_{i-1}}{\Delta t}$$

This expression is then used to compute n :

$$n = \frac{\bar{V}\dot{\gamma}}{g} + \cos \bar{\gamma}.$$

A more detailed breakdown of these methods is readily available from the authors upon request.

~~CONFIDENTIAL~~

APPENDIX III

A COMPARISON OF THE BRYSON-KELLEY AND THE MODIFIED RUTOWSKI TECHNIQUES

(U) In computing the path-dependent (variable fuel) E-ME and Range diagrams, a method is needed for computing the fuel consumed and horizontal distance traversed in flying from some reference point (h_0, M_0) to any point (h, M) inside the steady-state envelope of an aircraft. This implies some path connecting the points (h_0, M_0) and (h, M) in the altitude-Mach number plane. Of course, any number of "flyable" paths can be drawn which connect (h_0, M_0) and (h, M) . The foregoing E-M Efficiency and range considerations suggest a simplification by connecting (h_0, M_0) and (h, M) with a minimum fuel path.

(U) Use of a sophisticated technique, such as the one credited to Bryson and Kelley, becomes prohibitive because of the amount of computer time involved. For this reason, an approximate technique becomes exceedingly desirable.

(U) Heermann (Reference 3) observed that curves of constant minimum time are approximate curves of constant specific energy, E_s , in the altitude-Mach number plane. More recent investigations by Heermann indicate that the same is true for curves of constant minimum fuel.

(U) Heermann's results, coupled with experience gained with the Rutowski method, extended in the manner described in Appendix II, suggest that fuel consumed in traversing a Rutowski minimum fuel path to a given energy level is almost independent of the altitude-Mach number combination on that energy level. Additionally, for range computations, the horizontal distance traversed in climbing to a given altitude-Mach number point is small in comparison with the range remaining and, hence, a somewhat less accurate approximation of horizontal distance is acceptable.

(U) Investigations have revealed that the Rutowski approximations are extremely good ones. That is, in part, due to the fact that fuel and distance errors tend to compensate for each other.

(U) Numerous IBM 7094 computer runs for the F-4C and MIG-21 have been summarized and will be discussed here to support these remarks.

(C) The first example attests to the accuracy of the Rutowski approximation. It is a total path comparison for the F-4C from $M = 0.8$ at 100 feet to $M = 1.854$ at 44,900 feet ($E_s = 95,000$ feet), with an initial weight of 40,392 pounds. The Bryson-Kelley path indicated 4,017 pounds of fuel consumed and 68.4 nautical miles traversed, compared with 3,993 pounds of fuel consumed and 64.8 nautical miles traversed via the Rutowski program for the same case. A

[REDACTED]

difference of 2½ pounds (0.6%) and 3.6 miles (5.3%) exists between the Bryson-Kelley and the Rutowski paths. The Bryson-Kelley path required 92 minutes of computer time versus 1.4 minutes for the Rutowski path.

(U) The following cases illustrate the effects on fuel consumed and distance traversed when the terminal (h, M) lies above or below the Rutowski path at $E_s = 95,000$ feet. Since the subsonic portions of the paths for the F-4C were identical, only the supersonic portions were considered. The same statement applies to the MIG-21 paths. Figure II-1, page 46, indicates the general shape of the paths in the altitude-Mach number plane.

(S) Three Bryson-Kelley paths each were run for the F-4C and the MIG-21 from $M = 1.0$ at 39,000 feet and $M = 1.0$ at 44,700 feet, respectively, to $E_s = 95,000$ feet. Terminal conditions are given in Table III-1.

TABLE III-1. TERMINAL CONDITION DATA

Case	Aircraft	Altitude (ft)	Mach No.
1	F-4C	36,900	1.997
2	F-4C	44,900	1.854
3	F-4C	52,900	1.700
4	MIG-21	39,800	1.946
5	MIG-21	42,800	1.892
6	MIG-21	50,800	1.741

NASIC/ACAA
DECLASSIFY
(This information no longer needs to be classified)

(S) Cases 1, 2, and 3 terminated 8,000 feet below, on, and 8,000 feet above the Rutowski path at $E_s = 95,000$ feet, respectively. Cases 4, 5, and 6 terminated 3,000 feet below, on, and 8,000 feet above the Rutowski path at $E_s = 95,000$ feet, respectively. Placard constraints prevented the termination of case 4 below 39,800 feet.

(S) Table III-2 presents a comparison of the Bryson-Kelley and Rutowski paths. This table depicts fuel consumed for the Bryson-Kelley path, f_{BK} , and for the Rutowski path, f_R ; horizontal distance over the ground for the Bryson-Kelley path, x_{BK} , and for the Rutowski path, x_R . Also shown are the weight differences, ΔW , and percentage weight differences, $\% \Delta W$, between the Bryson-Kelley and Rutowski paths, as well as the distance differences, Δx , and percentage distance differences, $\% \Delta x$. All weights are in pounds, and all distances are in nautical miles.

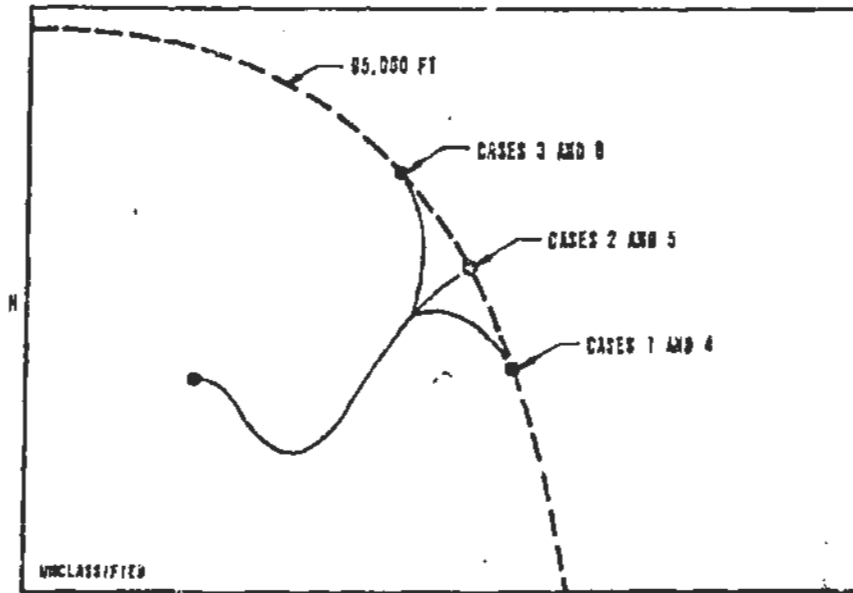


Figure III-1. Rutowski Path Comparison Scheme.

TABLE III-2. COMPARISON OF BRYSON-KELLEY AND RUTOWSKI PATHS

Case	Aircraft	f_{cBK}	f_{cR}	x_{BK}	x_R	Δw	$\% \Delta w$	Δx	$\% \Delta x$
1	F-4C	2350	-	47.8	-	28	1.2	2.8	5.9
2	F-4C	2372	2330	46.5	45.0	42	1.8	1.5	3.2
3	F-4C	2420	-	47.7	-	90	3.7	2.7	5.7
4	MIG-21	632	-	26.3	-	41	6.5	3.6	13.7
5	MIG-21	634	591	26.9	22.7	43	6.8	4.2	15.6
6	MIG-21	646	-	27.6	-	55	8.5	6.9	23.3

(U) Observation reveals that the fuel consumed via the Rutowski method is consistently less than the fuel consumed via the Bryson-Kelley method. The same consistency holds, however, for the horizontal distance traversed. The errors introduced by using this approximation technique tend to compensate for each other.

NASIC/ACAA
DECLASSIFY
(This information no longer needs to be classified)

[REDACTED]

(U) For the entire range computation, the percentage errors shown above become insignificant since the climb input is only a part of the total input. However, if more exact computations for the Range and L-M Efficiency diagrams are necessary, the Bryson-Kelley (or the Heermann) paths can be employed instead of the Rutowski paths.

REFERENCES

1. Rutowski, E. S., Energy Approach to the General Aircraft Performance Problem, Journal of Aeronautical Science, Volume 21, No. 3, March 1954.
2. Bryson, A. E. and Denham, W. F., A Steepest Ascent Method for Solving Optimum Programming Problems, Raytheon Company BR-2393, April 1963.
3. Heermann, H. and Kretzinger, P., The Minimum Time Problem, Journal of the Astronautical Sciences, Volume XI, No. 4, Winter 1964.
4. Boyd, John R., Aerial Attack Study, Nellis AFB 50-10-6c, Revised 11 August 1964.
5. Tactical Air Command Manual 3-1 (test), Counter Air Interdiction and Close Support, March 1965.
6. Dennison, J. M., Analytical Approach to F-4 Maneuvering in Air-to-Air Combat, McDonnell Aircraft Corporation B-163, 26 March 1965.
7. AIM-7D/AIM-7E Maneuvering Target and Minimum Range Definition Study, Raytheon Company, Missile Systems Division, BR 3361, 26 April 1965.
8. Boyd, John R. and Christie, Thomas P., Energy-Maneuverability Theory, APGC-TDR-64-35, May 1964.
9. Boyd, John R. and Christie, Thomas P., Energy-Maneuverability Theory and Applications, Paper for 12th Annual Air Force Science and Engineering Symposium, 9 October 1965.

~~88ABW/IPI
FOIA (b)(1) &
(b)(3)
10 USC 130~~

~~CONFIDENTIAL~~

Export Control

[This page is intentionally left blank.]

~~CONFIDENTIAL~~

~~CONFIDENTIAL~~


Export Control

[This page is intentionally left blank.]

~~CONFIDENTIAL~~

~~CONFIDENTIAL~~

Export Control

DEFENSE TECHNICAL INFORMATION CENTER 8725 JOHN J KINGMAN RD STE 0944 FT BELVOIR, VA 22060-6218					
OFFICIAL BUSINESS - PENALTY FOR PRIVATE USE, \$300 POSTMASTER: DO NOT FORWARD					
AD Number	Pages	Quantity	Type Copy	Source	Priority
AD372287	87	1 of 1	H	E	EXPRESS
Received Date: 31-MAR-11					
To: 87317					
Requested By: FOIA OFFICE					
Attn: Espinal, John					
AF Hq (IM10) FOIA Ofc 1000 Air Force Pentagon Rm 5C856 Washington, DC 20330-1000					
					868530001 

Distributed By **DTIC**
Information For The Defense Community

~~CONFIDENTIAL~~

20100413002